Basin Research
IAS EAGE

Sedimentary and thermal evolution of the Eocene-Oligocene mudrocks from the southwestern Thrace Basin (NE Greece)

Journal:	*Basin Research*
Manuscript ID:	BRE-045-2014.R2
Manuscript Type:	Original Article
Date Submitted by the Author:	n/a
Complete List of Authors:	Perri, Francesco; Università della Calabria, Dipartimento di Biologia, Ecologia e Scienze della Terra Caracciolo, Luca Cavalcante, Francesco Corrado, Sveva Critelli, Salvatore Muto, Francesco Dominici, Rocco
Keywords:	stratigraphy, geodynamics, basin subsidence

RUNNING TITLE: Sedimentary evolution of Thrace Basin mudrocks

Sedimentary and thermal evolution of the Eocene-Oligocene mudrocks from the southwestern Thrace Basin (NE Greece)

Perri F.*[1], Caracciolo L.[2], Cavalcante F.[3], Corrado S.[4], Critelli S.[1], Muto F.[1], Dominici R.[1]

[1]*Dipartimento di Biologia, Ecologia e Scienze della Terra, Università della Calabria, 87036 Rende (CS), Italy*

[2]*Chemostrat Ltd., Sandtrak Unit, Ravenscroft Court, Buttington Cross Enterpise, Welshpool, SY21 8SL, UK*

[3]*CNR – Istituto di Metodologie per l'Analisi Ambientale, 85050 Tito Scalo (PZ), Italy*

[4]*Dipartimento di Scienze, Sezione di Scienze Geologiche, Università degli Studi "Roma Tre", 00146 Roma, Italy*

*Corresponding author: Francesco Perri

Dipartimento di Biologia, Ecologia e Scienze della Terra,

Università della Calabria, 87036 Rende (CS), Italy

email: francesco.perri@unical.it

ABSTRACT

Paleothermal indicators based on clay mineral and organic matter analyses, were integrated with mudrock geochemistry and stratigraphic data to define the sedimentary evolution of the southwestern Thrace Basin during the Eocene to Oligocene periods. This multi-method approach allowed us to reconstruct the burial evolution of the basin in Eocene and Oligocene times and to study the mudrock composition and relate this to their provenance and source area weathering. The

studied mudrocks show similar chemical variations. The distribution of some major and trace elements for the studied samples reflect heterogeneous source areas containing both felsic to mafic rocks. In particular, the LREEs/TEs (Light Rare Earth Elements/Transition elements) ratios are very high for the Avdira and Organi samples (on the average between 1.5-2.2 for (La+Ce)/Cr and 3.5-8 for (La+Ce)/Ni), suggesting a felsic source(s), and very low for the Samothraki, Limnos, Paterma, and Iasmos samples (on the average between 0.4-0.6 for (La+Ce)/Cr and 0.6-1 for (La+Ce)/Ni), suggesting a mainly basic source(s). The mineralogical composition coupled with the A-CN-K and A-N-K plots suggest a complex evolution. The clay mineral data (illite percentage in I/S and the stacking order *R* and the Kübler Index) coupled to vitrinite reflectance analysis indicate a high to intermediate diagenetic grade for the Middle to Upper Eocene samples (from Iasmos, Gratini, Organi, Paterma, Esimi and Samotraki sections) and a low diagenetic grade for the Upper Eocene to Oligocene samples (from Limnos and Avdira sections). These data helped in interpreting the geodynamic evolution of the studied basins where the magmatic activity plays an important role. In particular, Middle to Upper Eocene sediments show high to intermediate diagenetic grade since they are located in a portion of the basin dominated by Eocene to Oligocene magmatic activity and intrusion of granitoids, whereas, the Upper Eocene to Oligocene sediments are not involved in important magmatic activity and intrusion of granitoids and, thus, show low diagenetic grade. Furthermore, Middle to Upper Eocene sediments experienced deeper burial processes caused by lithostatic load, rather than the uppermost Eocene and Oligocene sediments, in relation of their position along the stratigraphic succession. These data suggest a burial depth of at least 3–4 km with a tectonic exhumation mainly related to the extensional phases of the Miocene age.

INTRODUCTION

The studied area is located in the Aegean–Anatolia region which was affected by extensional tectonics since the Middle to Late Eocene and intrusion of several plutons and important faulting by several systems at the end of the Eocene (Jolivet *et al.*, 2013 and references therein). The Thrace Basin, one of the largest Tertiary basins in the North Aegean region, formed on top of the metamorphic rocks of the Rhodope Belt in northern Greece and the Strandja and Sakarya massifs in NW Turkey, where its depocentre developed. The area is characterized by important structural relationships among the Serbomacedonian Massif, Rhodope and Circum-Rhodope belts and the oceanic terranes constituting the Vardar-Axios suture, since they are involved in significant paleogeographical and paleotectonical modification related to the collision of the African and Eurasian plates (Fig. 1).

The sedimentary successions of the Thrace Basin are an important stratigraphic marker since they record the evolutionary path of the basin characterized by multi history tectonic assemblage. Therefore, the Thrace Basin represents an excellent area in which to investigate sedimentary processes, and the burial and final exhumation history during the evolutionary stages of the basin. The Rhodope Belt is mainly characterized by flat-lying thrusts developed during several compressional phases; it is successively exhumed during the Eocene-Miocene (e.g. Kilias *et al.*, 2011) following protracted extension beginning in the Late Eocene to Early Oligocene (e.g. Burchfiel *et al*., 2000; Bonev & Beccaletto, 2007). This extension is a general consequence of a collapse phase or the Hellenic accretionary prism (e.g. Platt, 1993; Kilias et al., 2011). The development of low-angle normal fault (e.g. detachment faults in Kilias et al., 2011) is coeval to the protracted convergence between the African and Eurasian plates (NNE-SSW oriented) combined with a retreat of the subduction zone towards the SW (e.g. Kilias et al., 2011 and references therein). The extension phases were accompanied by magmatism in the central-eastern and southern

Rhodope Belt, and a huge sedimentary accommodation within the Thrace Basin (e.g. Caracciolo *et al*., 2011). New mineralogical, geochemical, petrographic, and stratigraphic constraints of mudrocks of the sedimentary successions postdating the Oligocene cooling phase exposed in the northeastern Hellenic Peninsula along the western edge of the Thrace region have been analyzed in order to address this problem. Xray diffraction (XRD), Xray fluorescence (XRF), sedimentological, and organic matter optical analyses on these sedimentary successions were performed. Vitrinite reflectance (VRo%) and illite content in mixed-layer illite-smectite (%I in I-S), which are indicators of maximum paleotemperatures during diagenetic conditions (e.g. Pollastro, 1993; Aldega *et al.*, 2007; 2011; Carlini *et al.*, 2013), were used to define the paleothermal conditions.

In addition, sedimentological and tectono-stratigraphic studies associated with the distribution of major and trace elements, the mineralogical composition, and the organic matter data of the analyzed mudrocks, were used to reconstruct the sedimentary evolution of the southwestern Thrace Basin. In particular, the distribution of major and trace elements related to the mineralogical composition of clastic sediments is a useful tool to reconstruct the paleogeography and the paleotectonics of sedimentary basins and their relationships with the source area (e.g. Cullers, 2000, Critelli *et al.*, 2007, 2008; Zaghloul *et al.*, 2010; Perri *et al.*, 2008a; 2013; Perri and Ohta, 2014; Perri, 2014).

By combining the information deduced from the change in the X-ray diffraction (XRD) patterns after heating and ethylene glycol treatments and the elemental analyses for major and trace elements concentrations, it is possible to explain and predict the sedimentary evolution and geological processes affecting fine grained sediments and, thus, the relationship developed between the source area and sedimentary basin (e.g. Mongelli *et al.*, 2006; Critelli *et al.*, 2008, 2013; Zaghloul *et al.*, 2010; Caracciolo *et al.*, 2011a, 2011b, 2012, 2013a, 2013b; Perri *et al.*, 2011a; 2013).

GEOLOGICAL SETTING

The studied sedimentary successions are exposed in the northeastern Hellenic Peninsula along the southwestern edge of the Thrace Basin where structural relationships among Rhodope and Circum-Rhodope belts are exposed (Figs. 1 and 2). Closure of a series of oceanic basins, from the Middle to Late Mesozoic until the Late Eocene, led to development of the Rhodope accretionary complex (Barr *et al.*,1999; Cavazza *et al.*, 2004). The Rhodope Belt is mainly characterized by several thrusts developed during different compressional phases; it is successively exhumed during the Eocene and Miocene (e.g. Kilias *et al.*, 2011) following extensional phases starting from the Late Eocene to Early Oligocene (e.g. Burchfiel *et al*., 2000; Bonev & Beccaletto, 2007). Two main tectono-stratigraphic units have been recognised within the Rhodope Massif s.s.: a) the Lower Tectonic Unit (LTU) and b) the Upper Tectonic Unit (UTU). The Rhodope Massif is overlain and bordered to the southeast by a Mesozoic sequence, defined as the Circum-Rhodope Belt (Fig. 2). These units are locally unconformably overlain by unmetamorphosed Tertiary sedimentary and volcanic rocks. Finally, the youngest successions of the Thrace Basin are Late Miocene to Quaternary deposits (e.g. Meinhold & BouDagher-Fadel 2009; Kilias *et al.*, 2011; Caracciolo *et al.* 2011b, 2012; Cavazza et al., 2013).

The LTU includes the Sidironero, Kardamos and Kechros units and the UTU contains the Kimi Unit (Fig. 2). The LTU includes the Permo-Carboniferous granitoid protoliths and Permo-Triassic eclogite relics (Kozhoukharov *et al.,* 1988), marbles, and subordinate amphibolites constituting the core of the domes. U-Pb ages on zircons (Peytcheva & von Quadt 1995; Ovtcharova *et al.,* 2003; Carrigan *et al.,* 2003) and Rb/Sr (Mposkos & Wawrzenitz 1995) range from ca. 335 to 295 Ma testifying that the complex is attributable to a Variscan or older continental basement (Marchev *et al.,* 2004). The UTU (Barr *et al.*, 1999) is represented by a heterogeneous rock assemblage of mixed continental and oceanic affinity. It is composed of intercalated

metasedimentary (marbles, schists, and gneisses) and metaigneous (gabbros, plagiogranites, diorites) rocks, metaophiolites, and high-pressure cumulates (Haydoutov *et al.,* 2004). The ages of the protolith rocks have been recently constrained between Neoproterozoic (640 Ma), Ordovician (430–460 Ma), and Permian (290 Ma) which have experienced Carboniferous, likely Jurassic, and Tertiary metamorphic overprints (Carrigan *et al.,* 2003; Haydoutov *et al.,* 2004; Bonev *et al.,* 2010).

At the westernmost Rhodope massif, the Sidironero unit overthrusts the Pangaion unit (e.g. Kilias *et al.*, 2011). The Kechros-Kardamos Complex (Kozhoukharov *et al.*, 1988; Haydoutov *et al.*, 2004) includes the metamorphic units of continental origin known as the Lower Tectonic Unit (Barr *et al.*, 1999). It structurally represents the deepest level in the metamorphic basement, generally bordered on its top by extensional detachment faults and/or mylonitic shear zones. Geochronological data indicate that the complex is Variscan or older continental basement (Marchev *et al.*, 2004). Thermochronology documents cooling between 42 and 36 Ma, suggesting that metamorphism occurred before the Middle Eocene, between 73 and 45 Ma (Mukasa *et al.*, 2003 and references therein).

The Kimi Complex (Kozhoukharov *et al.*, 1988; Haydoutov *et al.*, 2004), contains remnants of oceanic and island-arc units and mainly consists of gneiss, amphibolite, marble, metagabbro, pelitic schist and rare quartzite; small bodies of ultramafic rocks are also present. Granitic bodies, intruding these rocks, have been dated using the U-Pb-zircon method at 70 Ma (Marchev *et al.*, 2004).

The Circum-Rhodope Belt (CRB) borders the southern Rhodope Massif. The CRB consists of Mesozoic low-grade metamorphic and meta-extrusive units, extending from Samothraki Island close to the Biga Peninsula (NW Turkey). These Mesozoic rocks commonly overlayed the crystalline basement as a nappe of wide regional extent (Bonev & Stampfli 2003). The entire sequence is represented by a basal greenschist unit overlain by mafic extrusive rocks of the Evros

ophiolite complex dated at 161 to 140 Ma by apatite fission-track ages on the mafic rocks (Bonev & Stampfli 2003). Both the CRB and the crystalline basement are overlain by Middle Eocene to Miocene sedimentary rocks. The Evros ophiolite, located in Thrace (NE Greece) belongs to the CRB; its age is considered to be Jurassic-Cretaceous (Bonev & Beccaletto, 2007 and references therein). Volcanic and pyroclastic rocks of tholeiitic composition are underlain by massive and pillow lavas with a few tuffaceous rocks and lava breccia in the upper ophiolitic sequence. Rocks of the CRB undergo intense deformation and low-grade metamorphism (Caracciolo *et al.*, 2011b). The tectonosedimentary evolution of the Rhodope region was synchronous with development of extensional processes and onset of a Tertiary magmatic orogenic belt bordering the southern European continental margin (e.g. Caracciolo *et al.*, 2011b). Remnants of the magmatic arc extend continuously from the Dinarides-Balkan to western Anatolia for more than 2000 km (Yanev *et al.*, 1998). Volcanic activity was initiated at 37 Ma in the Rhodope region, and it migrated south in western Anatolia and the central Aegean Sea until 15 Ma (Yanev *et al.*, 1998).

The Evros Basin

The Kirki-Esimi representative stratigraphic section of the Evros Basin has been studied in this work. The Kirki-Esimi section is characterized by a rapid subsidence that occurred during the Late Eocene to Oligocene, after deposition of Lutetian alluvial-fluvial, coarse sandstones and conglomerates. Rapid subsidence is indicated by deposition of marls, mudrocks and turbidite sandstone of outer shallow-marine and slope environments passing upward to a deep-marine turbidite succession of Late Eocene to Early Oligocene age. Lava flows and domes associated with volcanic agglomerates (Innocenti *et al.*, 1984) are interbedded with Oligocene deep-marine deposits. According to the Hellenic Institute of Geology and Mineral Exploration boreholes, the series is ca 250 m in thickness (e.g. Caracciolo *et al.*, 2011b).

The Kirki-Esimi section represents the base of the Evros Basin and includes the older sedimentary section in Southern Rhodopes. The sedimentary succession reaches a total thickness of 2000 m. The lower part of the Kirki-Esimi section can be interpreted as a braided river – alluvial fan system. The dominant sandstone facies involves an upward fining trend, which suggests a proximal-to-distal transition of alluvial-fan deposits interfingering with fluvial plain deposits. Conglomerate and sandstone are overlain by a gray-to-green silty succession about 500 m thick. At the top of the succession, dark gray siltstone is interbedded with decimetre thick paralic coal seams, suggesting the onset of a marine environment, characterized by a waning terrigenous supply and low oxygenation. The sedimentary succession continues with stratified carbonates, 80 to 100 m thick. In this section, poorly exposed carbonate strata consist of mostly limestone with corals, algae and nummulitidae, biocalcarenite and calcirudite. The carbonate section is here interpreted as an algal-coral patch reef. Overlying the carbonates is a 500 m thick slope of marls, sandstones, and deep marine turbidites (e.g. Caracciolo *et al.*, 2011b).

The Xanthi-Komotini basin

The Xanthi-Komotini basin is bounded by normal faults and exhibits a typical graben structure (e.g. Caracciolo *et al.*, 2011b). Basin asymmetry shows a regional south-eastward deepening related to the Kavala-Xanthi-Komotini fault (Tsokas *et al.*, 1996). The basin is bounded by the Avdira fault to the west and by the Circum-Rhodope Belt to the east. The sedimentary succession of the basin directly overlies on the crystalline basement of the Rhodope Massif, and ranges in age from Middle Eocene (Lutetian) to Neogene (e.g. Caracciolo *et al.*, 2011b).

Papadopulos (1982) proposed a Lutetian-Priabonian age for the entire Southern Rhodopes shallow-marine carbonate reef. Fossil assemblages in mudrock between the continental deposits and the shallow-marine carbonates consist of nummulites, miliolides, orbitolites and the planktic

foraminifera Morozovella sp. (Late Palaeocene – Middle Eocene) and Igorina sp., suggesting a middle Eocene age for the carbonate reef. However, data from benthic foraminifera, on coral reef packstone samples, indicate a Priabonian to Rupelian age, for the shallow-marine carbonates of the Avdira stratigraphic section, on the southern basin margin, suggesting that carbonate-reef sedimentation was protracted, reaching into the Late Eocene or possibly even into the Oligocene (e.g. Caracciolo *et al.*, 2011b).

The most representative stratigraphic section of the Xanthi-Komotini basin has been described in the vicinity of Iasmos, a village close to Xanthi. In this area, the basal sedimentary succession consists of continental coarse-grained sandstone and conglomerate of Lutetian age, overlain by Upper Eocene deep-water deposits capped by Oligocene fluvial conglomerate. The succession reaches a maximum thickness of 2000 m in the center of the basin (Tsokas *et al.*, 1996).

Northern Aegean basin

Limnos

The sedimentary succession at Limnos includes a continuous Middle-Upper Eocene through Lower Miocene succession, overlain and intruded by 21 to 18 Ma volcanic and sub-volcanic bodies (Igneous Complex) (Innocenti *et al.*, 1994, 2009).

Middle-Upper Eocene to Middle Oligocene deep-marine turbidite deposits, about 300 m thick, constitute the Fissini-Sardes Unit (e.g. Innocenti *et al.*, 1994; Caracciolo *et al.*, 2011b). The basal Fissini-Sardes Unit consists of a chaotic interval, including slump and olistostrome layers, the latter having 1 to 6 m diameter olistoliths of nummulitic limestone blocks. This basal interval is overlain by a ca 250 m thick sequence of turbidite sandstone and siltstone. In the lower parts of the turbidite sequence, a 6 m thick layer of tuff is interbedded with turbidite sandstone (e.g. Caracciolo *et al.*, 2011b). According to Innocenti *et al.* (1994), the faunal association indicates a Middle

Eocene (Lutetian) age. The Fissini-Sardes Unit is overlain by the Ifestia Unit, a 150 m thick marine sandstone, with up to 5 m of interbedded conglomerate and marl, which is Middle Oligocene to Lower Miocene in age. An erosional surface separates the Ifestia Unit from the Therma Unit. The Therma Unit reflects an abrupt change from marine to continental palaeoenvironments after a deformation and erosional phase that affected the turbidite strata. The unit consists of lenticular and channellised conglomerate strata, interbedded with marls, mudrocks and siliceous shales having abundant plant remains. Volcaniclastic sandstone strata are interbedded within the Therma Unit. Deposition of the Therma Unit predated onset of the main Early Miocene volcanic cycle of the Igneous Complex (e.g. Caracciolo *et al.*, 2011b).

Samothraki

Samothraki is situated in the northeast Aegean Sea and is generally considered as part of the Circum-Rhodope Belt (e.g. Tsikouras *et al.*, 1990). The oldest geological unit of the Circum-Rhodope Belt in the Samothraki predominantly consists of clastic sedimentary rocks metamorphosed up to greenschist facies, which are Late Jurassic to Early Cretaceous in age. They were deposited in a trench, deformed in an accretionary wedge, and later intruded by subduction related mafic to ultramafic rocks (Tsikouras *et al.* 1990) or accumulated in a continental-rift setting (Hatzipanagiotou & Tsikouras 2001). The mafic to ultramafic rocks mainly consist of gabbro, basalt, dolerite and diorite (e.g. Tsikouras & Hatzipanagiotou 1998; Hatzipanagiotou & Tsikouras 2001).

The rocks of the Circum-Rhodope Belt are locally unconformably overlain by unmetamorphosed Tertiary sedimentary and volcanic rocks. The western and eastern part of Samothraki is also characterized by Tertiary igneous rocks (e.g. Pe-Piper & Piper 2006, and references therein). The Tertiary volcanism in the northeastern Aegean region was related either to

the subduction of the Intra-Pontide Ocean (e.g. Pe-Piper & Piper 2006), or it was associated with crustal extension after the thickening/uplift of the Hellenic orogen as the result of under-thrusting of the African plate beneath the southern European margin (e.g. Christofides *et al.* 2004). The youngest successions on Samothraki are Late Miocene to Quaternary deposits (e.g. Meinhold & BouDagher-Fadel 2009).

SAMPLING AND METHODS

The studied mudrocks are from the southwestern Thrace Basin (Fig. 2) and collected in the Avdira (AVD1 and AVD3), Iasmos (IAS6, IAS7, IAS10, IAS12, IAS13 and IAS15), Gratini (GRD2), Organi (ORG4, ORG5 and ORG6), Paterma (PAT1, PAT4, PAT8 and PAT11), Esimi (ES5 and ES7; ES8 and ES11c only for the vitrinite reflectance analysis), Samotraki (SAMO10, SAMO28, SAMO29, SAMO30, SAMO32 and SAMO33; SAMO20 only for the vitrinite reflectance analysis) and Limnos (LMN2, LMN4, LMN9 and LMN13; LMN27 only for the vitrinite reflectance analysis) stratigraphic sections (Figs. 3 and 4). The studied area is characterized by sedimentary successions that can be subdivided into two main depocentres: Evros and Xanthi-Komotini. Figure 3 shows the synthetic and schematic stratigraphic sections of these two depocentres.

The mineralogy of the whole rock and fine fractions (<2 μm) was determined by X-ray powder diffraction (XRD) using a Rigaku D/max 2200 diffractometer (Cu-Kα radiation; graphite secondary monochromator; sample spinner; step size 0.02; speed 3sec for step). The <2 μm grain-size fraction was then separated by settling in distilled water. Oriented mounts were prepared, after Sr-saturation of the clay fraction (Eberl *et al.*, 1987), by evaporation of a clay-water suspension on the glass slides. X-ray diffraction analyses were carried out on air-dried specimens, glycolated at 60 °C for 8 hours, and heated at 375 °C for 1 hour (Moore & Reynolds, 1997).

Quantitative mineralogical analysis of the bulk rock was performed on random powders measuring peak areas using WINFIT computer program (Krumm,1996). The percentage of each mineral was obtained following the procedure proposed by Cavalcante *et al.* (2007).

The percentage of illite (%I) and stacking order (Reichweite; R) of the I-S mixed layers were determined on the spectrum of the glycolated specimen according to Moore & Reynolds (1997). The Kübler Index (KI; Kübler, 1967) was also determined for some samples (e.g. Perri *et al.*, 2011b; Cavalcante *et al.*, 2012 and reference therein). The assumptions used to estimate the thermobaric conditions of the investigated sedimentary rocks are from previous studies (e.g. Merriman & Peacor, 1999; Perri, 2008; Perri *et al.*, 2008b; 2011b; 2012a; 2013; Cavalcante *et al.*, 2012 and reference therein).

Elemental analyses for major and some trace elements (Nb, Zr, Y, Sr, Rb, Ba, Ni, Co, Cr, V) concentrations were obtained by X-ray fluorescence spectrometry (Bruker S8 Tiger) at the Università della Calabria (Italy), on pressed powder disks of whole-rock samples (prepared by milling to a fine grained powder in an agate mill) and compared to international standard rock analyses of the United States Geological Survey. Total loss on ignition (L.O.I.) was determined after heating the samples for three hours at 900 °C. The estimated precision and accuracy for trace element determinations are better than 5%, except for those elements having a concentration of 10 ppm or less. The latter are estimated to have 10 to15% precision and accuracy.

Vitrinite reflectance strictly depends on the thermal evolution of the hosting sedimentary rock and is correlated to the stages of hydrocarbon generation, coal rank and other thermal parameters in sedimentary environments (Durand, 1980), namely mineralogical indicators such as illite percentage in illite smectite mixed layers and Kübler Index (Merriman & Peacor, 1999). Thus it is the most widely used parameter to calibrate basin modeling in hydrocarbon exploration (Dow, 1977; Mukhopadhyay, 1994) and when used in association with other indicators, it turns out to be a

powerful tool for the reconstruction of the thermal evolution of sedimentary successions during diagenesis and anchizone (Aldega *et al.*, 2011; Corrado *et al.*, 2010, Izquierdo-Llavall *et al.* 2013). Furthermore vitrinite reflectance becomes anisotropic from maturity levels in the oil window (about 1%) and increases with increasing maturity. Thus, in organic diagenesis and catagenesis random reflectance (acronym R_o%) is generally used, whereas from metagenesis onward $R_o$max is generally preferred to describe levels of coalification.

In this work, mean random vitrinite reflectance (R_o%) was measured on whole-rock samples rich in coaly particles collected from sandstone, siltstone and clay lithologies. Samples were first mounted in epoxy resin and polished according to standard procedures (Bustin *et al.*, 1990). Vitrinite reflectance analyses were then performed on randomly oriented grains using a Zeiss Axioplan microscope and conventional microphotometric methods, under oil immersion (ne = 1.518) and an Epiplan-Neofluar 50x/1.0 oil objective in reflected monochromatic non-polarized light (lamba = 526 nm). Reflectance standards (with certified R_o% values of 0.4, 0.5, 0.9) were used for calibration. In most cases a population of a few tens of readings per sample were made on fragments only slightly fractured and/or altered (Borrego *et al.*, 2006). Mean reflectance and standard deviation values were calculated for all measurements identifying the indigenous population. Approximate paleo-temperatures were derived adopting Barker and Pawlewicz's equation (1994).

RESULTS

Whole-rock geochemistry

To better examine the geochemical features of the studied samples, the mudrock composition was normalized to standard PAAS shales (Post-Archaean Australian Shales; Taylor & McLennan, 1985) (Fig. 5a). The elemental concentrations and the ratios are given in Table 1.

According to the diagram of Herron (1988), the studied sediments fall in the shale field (Fig. 5b); among the mudrocks, only three SAMO samples fall in the Fe-shale field, since they are characterized by high concentrations of Fe-oxides, as shown by the mineralogical analyses.

The studied sediments show similar chemical variations relative to PAAS (Fig. 5a). Among the studied samples, AVD samples are enriched in Al oxide content and depleted in the other oxides. These samples contain higher kaolinite content than all the other samples as shown by mineralogical analyses on the clay fraction. Some SAMO samples contain the highest content in Fe oxides and transition elements (e.g. Ni and Cr); these concentrations suggest that these samples are related to mafic source(s).

Bulk rock composition

The results of whole rock XRD analyses are reported in Table 2. The non-phyllosilicate minerals are usually quartz, calcite, and feldspars. Some samples also contain hematite and dolomite. The phyllosilicates are generally illite, I-S and Chl-S mixed layers, chlorite, and kaolinite.

In detail, the ADV samples are characterized by mostly kaolinite with lesser amounts of feldspars, mica, chlorite, and Chl-S mixed layers. The ES samples contain mostly illite/mica and feldspars, whereas, the percentage of kaolinite is low. The GRD2 samples contain mostly illite/mica, I-S mixed layers, and calcite. Kaolinite is absent while feldspars and chlorite are low. The IAS samples contain mostly feldspars, whereas, calcite varies from 0 to 22%. Kaolinite and Chl-S mixed layers are low. The LMN group contains mostly illite/mica, chlorite, and calcite, whereas, the amount of Chl-S mixed layers and kaolinite is low. Quartz and illite/mica are abundant in OGR samples, but kaolinite, chlorite, and Chl-S mixed layers are absent. The PAT samples are characterized by variable amounts of phyllosilitates and calcite, whereas, the SAMO group contains mostly quartz, illite/mica, and chlorite. Hematite is also present in almost all samples.

Clay fraction composition

The <2 micrometer grain size fraction (Table 3) is mainly composed of I-S mixed layers (19-97% by weight). The highest values are contained in the ORG group. Chl-S mixed layers are present in variable amounts from 0 (AVD and ORG groups) up to 32% (SAMO group). This mineralogy is generally present in large amounts in the PAT and SAMO samples. Discrete illite is also variable, ranging from few percentage in the ADV group to 69% in the SAMO samples. It is also abundant in the PAT and LMN groups. Kaolinite is absent or present up to a few percent in most samples with the exception of the ADV samples. Chlorite is present in all samples and absent only in the ORG group.

As regard the illite percentage in I/S and the stacking order *R*, X-ray diffraction patterns of the glycolated oriented slides show the occurrence of the ordered R0 I/S mixed layers in the ADV and LMN samples (Figs. 6a and b). The percentage of illite is higher in the LMN samples. R1 characterizes the ES, GRD, PAT and SAMO groups (Figs. 6c, d, e and f) with the illite percentage ranging from 75% to 85%, but R3 with 85-90% of illite is present in the IAS and ORG samples (Figs. 6g and h). The KI is determined only in three samples: ES5 (0.45 °Δ2θ), ORG6 (0.56 °Δ2θ) and SAMO10 (0.44 °Δ2θ).

Organic petrography and vitrinite reflectance determination

Ten samples were analyzed for the characterization of the organic facies and evaluation of level of thermal maturity by means of R_o% measurement (Fig. 7). Only 7 out of 10 provided reliable values that can be correlated with other indicators of thermal exposure (e.g. %I and R number in illite-smectite mixed layers; KI) of the studied stratigraphic successions. The main results are summarized for each analyzed section.

One sample was analyzed (SAMO20) from the Eocene-Oligocene Samotracia section. It is quite rich in organic matter of probable continental origin (e.g. macerals of the inertinite group). Less abundant are macerals from the vitrinite group, sometimes intensely oxidized. R_o% of 0.70% is derived from a Gaussian distribution with a low standard deviation value (0.054). Sparse fragments with a random distribution of around 0.9 are also recorded and probably belong to reworked vitrinite populations. The approximate paleotemperature is of 107 °C is derived from the base of the indigenous population reflectance.

Two samples were analyzed (ORG5 and ORG6) from Upper Eocene-Oligocene Organi section. ORG5 is poor in organic matter with finely dispersed fragments of vitrinite group macerals that are clustered around the class 0.65%. Mean R_o% is 0.66 and higher values derived from scarce reworked fragments are discharged. The approximate paleotemperature is estimated to be 100 °C. Nevertheless the scarcity of fragments suggest a lower level of reliability of this sample when compared to those from the other sections. ORG6 is, as well, poor in organic matter, containing only rare fragments of inertinite group macerals not suitable for thermal maturity studies.

Two samples were studied (LMN27 and LMN13) from the Upper Eocene-Oligocene Limnos section. LMN13 is extremely rich in telinite and telocollinite that represent the prevalent fraction of its organic content with a good quality of preserved fragments that are distributed only into two frequency classes (0.35-0.40%). Ro% is of about 0.41% corresponding to an approximate paleo-temperature of 64 °C. LMN27, on the other end is barren.

From the Eocene Paterma section, PAT1 is an extremely well preserved. It is not oxidized, and it is rich in collinite and telocollinite fragments (macerals of the vitrinite group) that contain finely dispersed pyrite. Other macerals of the inertinite group are scarce and highly fractured. Measured fragments of the vitrinite group show a well-defined gaussian distribution with a R_o% of

about 1.0% with a low standard deviation value (0.09) indicating the mature stage of hydrocarbon generation with approximate paleotemperatures of around 135 °C.

IAS7 and IAS15 were analyzed from the Eocene Iasmos section. IAS7 is almost barren of dispersed organic matter and vitrinite group macerals are absent. Scarce fusinite fragments of the inertinite group are present, but cannot provide any contribution to the paleothermal study of the section. IAS15 is generally poor in organoclasts that are associated with well preserved and not oxidized pyrite framboids. Most of measurements are concentrated between 1.30 and 1.55% frequency classes and the Ro% is 1.42% indicating approximate paleotemperatures of about 164 °C.

Two samples were studied (ES8 and ES11c) from the Eocene Esimi section. ES8 is well preserved, not oxidized with huge fragments of vitrinite group macerals, containing finely dispersed pyrite, that prevail on other components. The Ro% of 0.92 is calculated from only one measured population of vitrinite fragments, presumably indigenous, testified by a slightly asymmetrical distribution of values. Approximate paleotemperatures are around 130 °C. The ES11c sample, despite being rich in organoclasts of the vitrinite group, is strongly oxidized and fragments are finely fractured. Thus the R_o% value of about 0.49% probably underestimates the effective reflectance despite a gaussian distribution of measurements.

DISCUSSION

Source area weathering and provenance

The content and distribution of the transition elements (e.g. Cr and Ni) and the LREEs (Light Rare Earth Elements; e.g. La and Ce) may provide useful indices of chemical differentiation that may allow the recognition of provenance (e.g. Perri *et al.*, 2012b and references therein), since their distributions are most similar to that found in the source rocks (e.g. Cullers *et al.*, 1987). The

distribution of major and trace elements (such as Fe, Mg, Cr and Ni, typical of a mafic source, and Al, Ti, La and Nb, typical of felsic source) for the studied samples, reflects heterogeneous source areas characterized by both felsic and mafic composition. The Cr/V *vs* Y/Ni diagram shows the curve model mixing between a granite (felsic member) and an ultramafic end member characterized by very low Y/Ni and high Cr/V ratio (Fig. 8a). In this diagram the studied samples fall along the curve model intermediate between ultramafic and felsic compositions, suggesting heterogeneous source areas characterized by both felsic and mafic composition (Fig. 8a). In particular, SAMO samples fall in the mixing curve between a felsic end-member and a mafic-ultramafic end-member, suggesting a provenance from mixing sources of both felsic and mafic composition. The contents and distributions of the LREEs (Light Rare Earth Elements; e.g. La and Ce) and the TE (Transition Elements such as Cr and Ni) may provide useful indices of chemical differentiation that may allow the recognition of different provenance areas (e.g. Cullers *et al.*, 1987; Perri *et al.*, 2012b). Low values of LREEs/TEs ratios generally reflect the greater input of mafic rocks with a modest felsic contribution (e.g. Perri *et al.*, 2012b and references therein). In particular, the LREEs/TEs ratios are very high for Avdira and Organi samples (on average between 1.5-2.2 for (La+Ce)/Cr and 3.5-8 for (La+Ce)/Ni), suggesting a greater input of felsic rocks, and very low for Samothraki, Limnos, Paterma and Iasmos samples (on average between 0.4-0.6 for (La+Ce)/Cr and 0.6-1 for (La+Ce)/Ni), suggesting a greater input of mafic-ultramafic rocks with a modest felsic contribution. Caracciolo *et alii* (2012) have also analyzed other elemental relationships (among La, Th and Sc) that confirm the above mentioned indications in terms of source(s) provenance of the studied successions. The mafic-ultramafic rocks could have been derived from the ophiolitic sequence of the Circum-Rhodope Belt, whereas, the felsic rocks could have been derived from granitoids intruding the LTU, the UTU, and the supradetachment basins (see Fig. 2) (e.g. Caracciolo *et al.*, 2011b; 2012; Cavazza *et al.*, 2013).

To better constrain the felsic versus mafic or ultramafic origin of the detritus, the V-Ni-La*6 ternary diagram (Fig. 8b), has been used that contains fields representative of felsic, mafic, and ultramafic rocks (e.g. Perri *et al.* 2011b). As a general rule, many of the studied samples plot close to the UCC and PAAS area, reflecting a felsic composition of source areas (Fig. 8b). The shifting of SAMO and LMN samples toward the V-Ni side suggests some mafic-ultramafic component in the detritus for these samples, as shown in the Cr/V *vs* Y/Ni diagram. Furthermore, some SAMO samples show the highest values of chlorite/smectite content, that is generally associated to mafic-ultramafic sources and, thus, confirms the patterns observed in the Cr/V *vs* Y/Ni and the V-Ni-La*6 diagrams that suggests mixing source(s) containing both felsic and mafic-ultramafic rocks.

The mineralogical composition, mainly characterized by variations in 10 Å-minerals (illite and micas), mixed layer phases, kaolinite and chlorite amounts, coupled with the A-CN-K and A-N-K (e.g. Nesbitt & Young, 1982; Perri *et al.*, 2014 and references therein) plots (Fig. 9a) and, thus, the CIA and CIA' distribution, suggest a complex evolution.

In this study both the CIA (Nesbitt & Young, 1982), with CaO values of the silicate fraction only (CaO content related to the carbonate minerals have been evaluated by XRD analysis), and the CIA' (e.g. Perri *et al.*, 2014), expressed as molar volumes of [Al/(Al+ Na+K)]x100 and, thus, calculated without the CaO content, have been used to monitor the source-area weathering. The studied samples are characterized by a linear trend subparallel to the A-CN join reflecting weathering from granitoid rocks, and a linear trend subparallel to the A-K join and plot near the A apex (Fig. 9a) reflecting the abundance of secondary clay minerals (e.g. kaolinite) over primary minerals (e.g. feldspars). The occurrence of variable amount of labile minerals in studied rocks corresponds to a variable degree of weathering in the source terrain. The CIA values (ranging from 56 to 77) of the studied samples generally indicate moderate chemical weathering of the source rocks; only the Avdira samples (average CIA value of 86) contain values that may be ascribed to

moderate/intense chemical weathering. The higher values of AVD samples are anticipated because of the increased production of aluminous minerals during chemical weathering, as also shown in the mineralogical analyses. The observed trends may be related to (1) different source areas characterized by different conditions of weathering rates, (2) different conditions of balance between physical (tectonism/uplift/erosion) and chemical processes. The active tectonism is related to Paleogene to Neogene extension of the Rhodope Massif and formation of the Paleogene volcano-sedimentary Thrace Basin (see Fig. 1) on top of the Paleogene extensional detachment fault system, simultaneously with uplift of deep crustal metamorphic Rhodope units (Fig. 10) (e.g. Kilias *et al.*, 2011; 2013 and references therein). The geometry and kinematics of deformation, cross-cutting relationships, kinematic indicators and slickenslides overprinting criteria on the fault planes discriminate five (D1 to D5) tectonic events (Kilias *et al.*, 2011; 2013). They took place from the Middle–Late Eocene to the present and are related to the basin evolution and the unroofing of the Rhodope metamorphic units (Kilias *et al.*, 2011; 2013). In particular, during the Eocene to Miocene, the key tectonic events are mainly characterized by ductile and brittle conditions that take place simultaneously at several tectonic crustal levels, whereas the Miocene through recent tectonic events are mainly characterized by brittle conditions (e.g. Kilias *et al.*, 2011; 2013).

Furthermore, paleoclimatic variations may be taken into account since the studied sediments have different ages of formation. The AVD samples are Oligocene in age, but the other samples are Eocene; thus, different paleoclimatic conditions characterize the transition from Eocene to Oligocene, where a humid climate favours the formation of kaolinite-rich levels (characterizing the AVD samples, as shown by mineralogical analyses on the clay fraction).

The data collected from geochemical analyses on the mudrock samples indicate a different composition of the source area(s) related to: 1) felsic and mafic sources that supplied the

sedimentary basin; 2) felsic and mafic sources eroded at different times following the uplift processes, as mentioned above.

The A-CN-K and A-N-K diagrams are used to predict chemical weathering intensity and variation of mineralogical or geochemical components through alkalis and Al content but fails to reflect migration or weathering of other elements. The coefficients of variability (CV) in Fe, Mg and Ti are relatively high and these elements generally show a positive correlation, indicating that Fe and Mg have gone through significant differential weathering or migration processes. The A-CNK-FM pattern is used to show variations in Fe and Mg abundances (Nesbitt & Young, 1996). Total Fe and Mg contents (FM value; Fig. 9b) vary significantly and show a decreasing trend for SAMO and PAT samples especially, while Al and other alkalis have slightly increases. Thus, this diagram shows that some SAMO and PAT samples are characterized by abundant ferromagnesian minerals. Furthermore, the two trends observed in the A-CNK-FM diagram (Fig. 9b) suggest that a mixing source, characterized by both felsic and mafic rocks, supplies the sedimentary basins where the studied sediments have been deposited.

The Index of Compositional Variability (ICV; Cox *et al.*, 1995) values for the studied samples are >1, typical of terrigenous sedimentary rocks that tend to occur in first-cycle deposits and in an area characterized by tectonic uplift, as shown above. The studied samples are not-affected by evident recycling processes, as shown by the Al-Zr-Ti diagram, and are less mature mudrocks. The Al-Ti-Zr ternary diagram monitors the effects of sorting processes (Garcia *et al.*, 1994). On this diagram (Fig. 9c), mature sediments consisting of both sandstones and shales show a wide range of TiO_2/Zr variations whereas immature sediments of sandstones and shales show a more limited range of TiO_2/Zr variations. On the Al-Ti-Zr diagram, the studied sediments are confined in the center with a limited range of TiO_2/Zr variations, suggesting poor sorting and rapid deposition of the sediments. All these observations support deposition in sedimentary basins close

to source areas containing both felsic and mafic rocks in a tectonically active setting and suggest that relief and rate of mechanical erosion were significant.

Diagenetic grade and thermal history

There is a broad consensus in the literature about the hypothesis that smectite-to-illite conversion is a progressive trend mainly controlled by temperature (see Merriman and Peacor, 1999; Árkai, 2002; Merriman, 2005; and reference therein). Other variables that may influence the process are time (Pytte & Reynolds, 1989; Pollastro, 1993), K-availability (e.g. Moore & Reynolds, 1997; Weibel, 1999; Cavalcante *et al.*, 2007; Somelar *et al.*, 2009) and fluid circulation (Eslinger & Pevear, 1988).

The presence of I/S R0 and the lowest content of illite in AVD and LMN samples suggest these groups formed at the lowest diagenetic grade, indicating a temperature range of 50 to 100 °C. This rough estimate is confimed and refined at least for the LMN section where Ro% of about 0.41% corresponds to an approximate paleo-temperature of 64 °C. The R1 I-S mixed layers with the illite percentage ranging from 75 to 85% determined in the ES, GRD, PAT and SAMO sections suggest an intermediate diagenetic grade of T = 100 to 130 °C. This is confirmed by vitrinite reflectance analysis at least for the ES, PAT and SAMO sections in which the approximate paleotemperatures are of about 130 °C, 135 °C and 107 °C, respectively. The ES5 and SAMO10 samples show KI values slightly lower than the diagenetic-anchizone boundary. This could be in accordance with a higher K-availability thus explaining the large amount of discrete illite. R3 containing 85 to 90% of illite is determined in the IAS and ORG samples, indicating a high diagenetic grade with temperatures ranging from 120 to 160 °C in accordance with the KI value (0.56 °$\Delta 2\theta$) measured in ORG6. This is only partially strengthened by organic matter analysis as the IAS section shows paleotemperatures of about 160 °C, whereas lower values are indicated for the ORG section.

Nevertheless, the ORG level of thermal maturity must be considered less reliable than those from other sections because of the scarcity of measured indigenous vitrinite fragments. Moreover, the ORG samples contain a high K_2O content; this K-availability may be influence the illitization of smectite as suggested by some authors (e.g. Cavalcante *et al.*, 2007).

Samples showing the highest to intermediate diagenetic grade (IAS, ORG, ES, GRD, PAT and SAMO respectively) are all Middle to Upper Eocene in age, whereas those exhibiting the lowest diagenetic grade (LMN and AVD) are Upper Eocene to Oligocene in age.

These data need to be interpreted according to the magmatic activity and geodynamic evolution of the basin during the Eocene to Oligocene periods (see Fig. 1). In particular, Middle to Upper Eocene sediments (IAS, ORG, ES, GRD, PAT and SAMO respectively) are located in a portion of the basin dominated by magmatic activity and intrusion of granitoids whereas the Upper Eocene to Oligocene sediments (LMN and AVD) are not associated with significant magmatic activity and intrusion of plutonic body (granitoids) (see Fig. 10). Furthermore, ES5 and SAMO10, showing KI values slightly lower than the diagenetic-anchizone boundary, are the samples located at the base of the succession; thus, the high lithostatic/tectonic load and the deformation processes occurred during the Eocene compressional phases, produced lower KI values in the lowest samples typical of high degrees of diagenesis. At the same time, LMN and AVD, showing the I/S R0 and the lowest content of illite typical of low to intermediate diagenetic grade, are the samples collected at the top of the studied succession and are Upper Eocene to Oligocene in age when deformation was less active with a phase of relative tectonic quiescence (e.g. Georgiev *et al.*, 2010). The IAS, ORG and PAT samples generally show I/S R1 and R3 with 80-90% of illite, and the ORG6 sample is further characterized by low KI values typical of high degrees of diagenesis generally related to the magmatic activity and geodynamic evolution of the basin during the Eocene to Oligocene periods. These samples are further characterized by the highest potassium contents. Thus, R1 and R3 values

for the I/S mixed layers may be also related to the K-availability characterizing this part of the studied succession.

CONCLUSIONS

The Thrace Basin is an area where important tectono-stratigraphic relationships among the Serbomacedonian Massif, Rhodope and Circum-Rhodope belts and the oceanic terranes of the Vardar-Axios suture, since they are involved in significant paleogeographical and paleotectonical modification related to the collision of the African and Eurasian plates. Thus, the evolution of the Thrace Basin plays an important role to better understand the geodynamic context of the Hellenides, in terms of source area(s) provenance and sedimentary and thermal history of the basin. The studied mudrocks were collected from different sedimentary successions exposed in the north-eastern Hellenic Peninsula along the western edge of the Thrace region.

The mineralogical composition, mainly characterized by variations in 10 Å-minerals (illite and micas), mixed layer phases, kaolinite and chlorite amounts, coupled with the geochemical proxies, suggest a complex evolution for these sedimentary successions. The data collected from geochemical investigations on the mudrock samples indicate a different composition of the source area(s) related to: 1) both felsic and mafic sources that supplied the sedimentary basin and 2) felsic and mafic sources eroded in different times following the uplift processes, such as the extensional detachment fault systems characterizing the basin during the Eocene and Oligocene periods.

The clay mineral data, based on illite percentage in I/S and the stacking order *R* and the Kübler Index, integrated with the Ro% values obtained from the vitrinite reflectance analysis, indicates a high to intermediate diagenetic grade for the Middle to Upper Eocene samples (IAS, ORG, ES, GRD, PAT and SAMO respectively) and a low diagenetic grade for the Upper Eocene to Oligocene samples (LMN and AVD). These variations need to be interpreted according to the magmatic

activity and geodynamic evolution of the basin during the Eocene and Oligocene periods. In particular, Middle to Upper Eocene sediments (IAS, ORG, ES, GRD, PAT and SAMO respectively) are located in a portion of the basin dominated by (Eocene to Oligocene) magmatic activity and intrusion of granitoids whereas the Upper Eocene to Oligocene sediments (LMN and AVD) are not related to magmatic activity and intrusion of the granitoids. Furthermore, Middle to Upper Eocene sediments experienced deeper burial process due to lithostatic load, rather than the uppermost Eocene and Oligocene sediments, in relation of their position along the stratigraphic succession. These data suggest a burial depth of at least 3–4 km with a tectonic exhumation mainly related to the extensional phases of the Miocene age.

ACKNOWLEDGMENTS

This research has been carried out within the MIUR-ex60% Projects (Relationships between Tectonic Accretion, Volcanism and Clastic Sedimentation within the Circum-Mediterranean Orogenic Belts, 2006–2013; Resp. S. Critelli), the 2009 MIURPRIN Project 2009PBA7FL_001 ‘The Thrace sedimentary basin (Eocene-Quaternary) in Greece and Bulgaria: stratigraphic depositional architecture and sediment dispersal pathway within post-orogenic basins.’ (Resp. S. Critelli). The authors are indebted to Manuel Martín-Martín and Robert L. Cullers and the Editor Cynthia J. Ebinger for their reviews and suggestions on an earlier version of the manuscript.

REFERENCES

ALDEGA, L., CORRADO, S., GRASSO, M. & MANISCALCO, R. (2007) Correlation of diagenetic data from organic and inorganic studies in the Apenninic-Maghrebian fold-and-thrust belt: A case study from eastern Sicily. *Journal of Geology*, 115, 335–353.

ALDEGA, L., CORRADO, S., DI PAOLO, L., SOMMA, R., MANISCALCO, R. & BALESTRIERI, M.L., (2011) Shallow burial and exhumation of the Peloritani Mts. (NE Sicily, Italy): Insight from paleo-thermal and structural indicators. *GSA Bulletin*, 123, 132-149.

ÁRKAI, P. (2002) Phyllosilicates in very low-grade metamorphism: transformation to micas. In: *Micas: crystal chemistry and metamorphic petrology* (Ed. By A. Mottana, F.P. Sassi, J.B., Thomson and S. Guggenheim). *Reviews in Mineralogy and Geochemistry*, 46, 463-478. Mineralogical Society of America.

BARKER, C.E. & PAWLEWICZ, M.J. (1994) Calculation of vitrinite reflectance from thermal histories and peak temperatures: a comparison of methods. In: *Vitrinite reflectance as a maturity parameter: applications and limitations* (Ed. By P.K. Mukhopadhyay and W.G. Dow). *ACS Symposium Series* 570, 216–229.

BARR, S.R., TEMPERLEY, S. & TARNEY, J. (1999) Lateral growth of the continental crust through deep level subduction-accretion: a re-evaluation of central Greek Rhodope. *Lithos*, 46, 69–94.

BONEV, N. & BECCALETTO, L. (2007) From syn- to post-orogenic Tertiary extension in the north Aegean region: constraints on the kinematics in the eastern Rhodope-Thrace, Bulgaria-Greece and the Biga peninsula. In: *The Geodynamics of the Aegean and Anatolia* (Eds T. Taymaz, Y. Yilmaz and Y. Dilek,) *Geol. Soc. Lond. Spec. publ.,* 291, 113-142.

BONEV, N.G. & STAMPFLI, G.M. (2003) New structural and petrologic data on Mesozoic schists in the Rhodope (Bulgaria): geodynamic implications. *CR Geosciences*, 335, 691–699.

BONEV, N., SPIKINGS, R., MORITZ, R. & MARCHEV, P. (2010) The effect of early Alpine thrusting in late-stage extensional tectonics: evidence from the Kuilidzhik nappe and the Pelevun extensional allochton in the Rhodope Massif, Bulgaria. *Tectonophysics,* 48, 256–281.

BORREGO, A.G., ARAUJO, C.V., BALKE, A., CARDOTT, B., COOK, A.C., DAVID, P., FLORES, D., HÀMOR-VIDÒ, M., HILTMA NN, W., KALKREUTH, W., KOCH, J., KOMMEREN, C.J., KUSC, J., LIGOUIS, B., MARQUES, M., MENDONC¸AFIL HO, J.G., MISZ, M., OLIVEIRA, L., PICKEL, W., REIMER, K., RANASINGHE, P., SUÀREZ-RUIZ, I. & VIETH, A. (2006) Influence of particle and surface quality on the vitrinite reflectance of dispersed organic matter: comparative exercise using data from the qualifying system for reflectance analysis working group of ICCP. *International Journal of Coal Geology*, 68, 151-170.

BURCHFIEL, C.B., NAKOV, R., TZANKOV, T. & ROYDEN, L.H. (2000) Cenozoic extension in Bulgaria and northern Greece: the northern part of the Aegean extensional regime. In: *Tectonics and Magmatism in Turkey and Surrounding Area.* (Eds E. Bozkurt, J.A. Winchester and J.D.A. Piper), *Geol. Soc. London Spec. Publ.*, 173, 325–352.

BUSTIN, R. M., BARNES, M. A. & BARNES, W. C. (1990) Determining levels of organic diagenesis in sediments and fossil fuels, in: McIleareath, I. A., Morrow, D.W., (Eds.), Diagenesis. St. John's, Geol. Assoc. Can. pp. 205–226.

CARACCIOLO, L., LE PERA, E., MUTO, F. & PERRI, F. (2011a) Sandstone petrology and mudstone geochemistry of the Peruc-Korycany Formation (Bohemian Cretaceous Basin, Czech Republic). *International Geology Review*, 53, 1003-1031.

CARACCIOLO, L., CRITELLI, S., INNOCENTI, F., KOLIOS, N. & MANETTI, P. (2011b) Unravelling provenance from Eocene-Oligocene sandstones of the Thrace Basin, North-east Greece. *Sedimentology* 58, 1988-2011.

CARACCIOLO, L., CRITELLI, S., INNOCENTI, F., KOLIOS, N. & MANETTI, P. (2013a) Unravelling provenance from Eocene-Oligocene sandstones of the Thrace Basin, North-east Greece: Discussion and Reply. *Sedimentology* 60, 865-869.

CARACCIOLO, L., VON EYNATTEN, H., TOLOSANA-DELGADO, R., CRITELLI, S., MANETTI, P. & MARCHEV, P. (2012) Petrological, geochemical, and statistical analysis of eocene-oligocene sandstones of the western Thrace basin, Greece and Bulgaria. *Journal of Sedimentary Research*, 82, 482-498.

CARACCIOLO, L., GRAMIGNA, P., CRITELLI, S., CALZONA, A.B. & RUSSO F. (2013b) Petrostratigraphic analysis of a Late Miocene mixed siliciclastic-carbonate depositional system (Calabria, Southern Italy): implications for Mediterranean paleogeography. *Sedimentary Geology*, 284, 117-132.

CARLINI, M., ARTONI, A., ALDEGA L., BALESTRIERI, M.L., CORRADO, S., VESCOVI, P., BERNINI, M. & TORELLI, L. (2013) Exhumation and reshaping of far-travelled/allochthonous tectonic units in mountain belts. New insights for the relationships between shortening and coeval extension in the western Northern Apennines (Italy). *Tectonophysics*, 608, 267-287.

CARRIGAN, C., MUKASA, S., HAYDOUTOV, I. & KOLCHEVA, K. (2003) Ion microprobe U–Pb zircon ages of pre-Alpine rocks in the Balkan, Sredna Gora, and Rhodope terranes of Bulgaria: constraints on Neoproterozoic and Variscan tectonic evolution. *J. Czech Geol. Soc.,* 48, 32–33.

CAVALCANTE, F., BELVISO, C., LAURITA, S. & PROSSER, G. (2012) P-T constraints from phyllosilicates of the Liguride Complex of the Pollino area (Southern Apennines, Italy): Geological inferences. *Ofioliti*, 37, 65-75.

CAVALCANTE, F., FIORE, S., LETTINO, A., PICCARRETA, G. & TATEO, F. (2007) Illite-Smectite mixed layer in Sicilide shales and piggy-back deposits of the Gorgoglione Formation (Southern Apennines): Geological inferences. *Bollettino della Società Geologica Italiana*, 103, 241 -254.

CAVAZZA, W., CARACCIOLO, L., CRITELLI, S., D'ATRI, A. & ZUFFA, G.G. (2013) Petrostratigraphic evolution of the Thrace Basin (Bulgaria, Greece, Turkey) within the context of Eocene-Oligocene post-collisional evolution of the Vardar-İzmir-Ankara suture zone. *Geodinamica Acta* 26, 12-26.

CAVAZZA, W., ROURE, F., SPAKMAN, W., STAMPFLI, G.M. & ZIEGLER, A. (2004) The TRANSMED Atlas, the Mediterranean Region From Crust to Mantle. Springer, Berlin, 141 pp.

CHRISTOFIDES, G., PECSKAY, Z., ELEFTHERIADIS, G., SOLDATOS, T. & KORONEOS, A. (2004) The Tertiary Evros volcanic rocks (Thrace, Northeastern Greece): Petrology and K/Ar geochronology. *Geologica Carpathica* 55, 397-409.

CORRADO, S., INVERNIZZI, C., ALDEGA, L., D'ERRICO, M., DI LEO, P., MAZZOLI, S. & ZATTIN, M. (2010) Testing the validity of organic and inorganic thermal indicators in different tectonic settings from continental subduction to collision: the case history of the Calabria-Lucania border (southern Apennines, Italy). *Journal of Geological Society* 167, 985-999.

COX, R., LOWE, D.R. & CULLERS, R.L. (1995) The influence of sediment recycling and basement composition on evolution of mudrock chemistry in southwestern United States. *Geochimica et Cosmochimica Acta* 59, 2919–2940.

CRITELLI, S., LE PERA, E., GALLUZZO, F., MILLI, S., MOSCATELLI, M., PERROTTA, S. & SANTANTONIO, M. (2007) Interpreting siliciclastic-carbonate detrital modes in Foreland Basin Systems: an example from Upper Miocene arenites of the Central Apennines,

Italy, in: Arribas, J., Critelli, S. & Johnsson, M.,(Eds.), Sedimentary Provenance: Petrographic and Geochemical Perspectives. Geological Society of America Special Paper 420, 107-133.

CRITELLI, S., MONGELLI, G., PERRI, F., MARTÌN-ALGARRA, A., MARTÌN-MARTÌN, M., PERRONE, V., DOMINICI, R., SONNINO, M. & ZAGHLOUL, M.N. (2008) Compositional and geochemical signatures for the sedimentary evolution of the Middle Triassic–Lower Jurassic continental redbeds from Western-Central Mediterranean Alpine Chains. *Journal of Geology* 116, 375-386.

CRITELLI, S., MUTO, F., TRIPODI, V. & PERRI, F. (2013) Link between thrust tectonics and sedimentation processes of stratigraphic sequences from the southern Apennines foreland basin system, Italy. *Rendiconti Online della Società Geologica Italiana* 25, 21-42.

CULLERS, R.L. (2000) The geochemistry of shales, siltstones and sandstones of Pennsylvanian–Permian age, Colorado, USA: implications for provenance and metamorphic studies. *Lithos* 51, 181–203.

CULLERS, R.L., BARRETT, T., CARLSON, R. & ROBINSON, B. (1987) Rare-earth element and mineralogic changes in Holocene soil and stream sediment: a case study in the West Mountains, Colorado, U.S.A. *Chemical Geology* 70, 335–348.

DOW, W.G. (1977) Kerogen studies and geological interpretation. *Journal of Geochemical Exploration* 7, 79–99.

DURAND, B. (1980) Sedimentary organic matter and kerogen. Definition and quantitative importance of kerogen, in: Durand, B., (Ed.), Kerogen: Insoluble Organic Matter from Sedimentary Rock. Paris, Edit. Technip, pp. 13–34.

EBERL, D.D., ŚRODOŃ, J., LEE, M., NADEAU, P.H. & NORTHROPO, H.R. (1987) Sericite from the Silverton caldera: Correlation among structure, composition, origin, and particle thickness. *American Mineralogy* 72, 914-934.

ESLINGER, E. & PEVEAR, D. (1988) Clay minerals for petroleum geologists and engineers. Short Course No. 22, SEPM, Society for Sedimentary Geology, Tulsa, USA.

GARCÍA, D., FONTEILLES, M. & MOUTTE, J. (1994) Sedimentary fractionations between Al, Ti, and Zr and the genesis of strongly peraluminous granites. *Journal of Geology* 102, 411-322.

GEORGIEV, N., PLEUGER, J., FROITZHEIM, N., SAROV, S., JAHN-AWE, S. & NAGEL, T.J. (2010) Separate Eocene–Early Oligocene and Miocene stages of extension and core complex formation in the Western Rhodopes, Mesta Basin, and Pirin Mountains (Bulgaria). *Tectonophysics* 487, 59-84.

HATZIPANAGIOTOU, K. & TSIKOURAS, B. (2001) Rodingite formation from diorite in the Samothraki ophiolite, NE Aegean, Greece. *Geological Journal* 36, 93-109.

HAYDOUTOV, I., KOLCHEVA, K., DAIEVA, L.A., SAVOV, I. & CARRIGAN, C.H. (2004) Island arc origin of the Variegated Formations from the East Rhodope, Bulgaria – implications for the evolution of the Rhodopes Massif. *Ofioliti* 29, 145–157.

HERRON, M.M. (1988) Geochemical classification of terrigenous sands and shales from core or log data. *Journal of Sedimentary Petrology* 58, 820–829.

INNOCENTI, F., KOLIOS, N., MANETTI, P., MAZZUOLI, R., PECCERILLO, A., RITA, F. & VILLARI, L. (1984) Evolution and geodynamic significance of the Tertiary orogenic volcanism in northeastern Greece. *Bulletin of Volcanology* 47, 25–37.

INNOCENTI, F., MANETTI, P., MAZZUOLI, R., PERTUSATI, P., FYTIKAS, M. & KOLIOS, N. (1994) The geology and geodynamic significance of the Island of Limnos, North Aegean sea, Greece. *Neues Jahrbuch für Geologie und Paläontologie* 11, 661–691.

INNOCENTI, F., MANETTI, P., MAZZUOLI, R., PERTUSATI, P., FYTIKAS, M., KOLIOS, N., VOUGIOUKALAKIS, G.E., ANDROULAKAKIS, N., CRITELLI, S. &

CARACCIOLO, L. (2009) Geological map (scale 1:50,000) of Limnos Island (Greece): explanatory notes. *Acta Vulcanologica* 20, 87–97.

IZQUIERDO-LLAVALL, E., ALDEGA, L., CANTARELLI, V., CORRADO, S., GIL-PEÑA, I., INVERNIZZI, C. & CASAS, A.M. (2013) On the origin of cleavage in the Central Pyrenees: Structural and paleo-thermal study. *Tectonophysics* 608, 303-318.

JOLIVET, L., FACCENNA, C., HUET, B. *et al.* (2013) Aegean tectonics: Strain localisation, slab tearing and trench retreat. *Tectonophysics* 597, 1–33.

KILIAS, A., FALALAKIS, G., SFEIKOS, A., PAPADIMITRIOU, E., VAMVAKA, A. & GKARLAOUNI, C. (2011) Architecture of Kinematics and Deformation History of the Tertiary Supradetachment Thrace Basin: Rhodope Province (NE Greece), in : Schattner, U., (Ed.) New Frontiers in Tectonic Research - At the Midst of Plate Convergence. InTech Publisher, Croatia, pp. 241-268.

KILIAS, A., FALALAKIS, G., SFEIKOS, A., PAPADIMITRIOU, E., VAMVAKA, A. & GKARLAOUNI, C. (2011) The Thrace basin in the Rhodope province of NE Greece – A tertiary supradetachment basin and its geodynamic implications. *Tectonophysics* 595-596, 90-105.

KOZHOUKHAROV, D., KOZHOUKHAROVA, E. & PAPANIKOLAOU, D. (1988) Precambrian in the Rhodope Massif, in: Zoubek, V., (Ed.), Precambrian in Younger Fold Belts. John Wiley and Sons, Chichester, pp. 723–778.

KRUMM, S. (1996) WINFIT 1.2: version of November 1996 (The Erlangen geological and mineralogical software collection) of "WINFIT 1.0: a public domain program for interact ive profile-analysis under WINDOWS". XIII Conference on Clay Mineralogy and Petrology, Praha, 1994. Acta Univers itatis Carolinae Geologica, 38, 253 –261.

KÜBLER, B. (1967) La cristallinité de l'illite e les zones tout a fait supérieures du métamorphisme, in: Etages tectoniques. Colloque de Neuchatel, 1996, Univ. Neuchate, 105-121.

MARCHEV, P., RAICHEVA, R., DOWNES, H., VASELLI, O., CHIARADIA, M. & MORITZ, R. (2004) Compositional diversity of Eocene–Oligocene basaltic magmatism in the Eastern Rhodopes, SE Bulgaria: implications for genesis and tectonic setting. *Tectonophysics* 393, 301–328.

MEINHOLD, G. & BOUDAGHER-FADEL, M. (2009) Geochemistry and biostratigraphy of Eocene sediments from Samothraki Island, NE Greece. *Neues Jahrbuch für Geologie und Paläontologie* 256, 17–38.

MERRIMAN, R.J. (2005) Clay minerals and sedimentary basin history. *European Journal of Mineralogy* 17, 7-20.

MERRIMAN, R.J. & PEACOR, D.R. (1999) Very low-grade metapelites: mineralogy, microfabrics and measuring reaction progress, in: Frey, M., Robinson, D., (Eds.), Low-Grade Metamorphim, Blackwell Scienze, Oxford, pp. 10-60.

MCLENNAN, S.M., TAYLOR, S.R. & HEMMING, S.R. (2006) Composition, differentiation, and evolution of continental crust: constrains from sedimentary rocks and heat flow, in: Brown, M., Rushmer, T. (Eds.), Evolution and Differentiation of the Continental Crust. Cambridge University Press, Cambridge, pp. 92–134.

MONGELLI, G., CRITELLI, S., PERRI, F., SONNINO, M. & PERRONE, V. (2006) Sedimentary recycling, provenance and paleoweathering from chemistry and mineralogy of Mesozoic continental redbed mudrocks, Peloritani Mountains, Southern Italy. *Geochemical Journal* 40, 197-209.

MOORE, D.M. & REYNOLDS, R.C. (1997) X-ray diffraction and identification and analysis of clay minerals. Oxford University press, Oxford.

MPOSKOS, E. & WAWRZENITZ, N. (1995) Metapegmatites and pegmatites bracketing the time of high P-metamorphism in polymetamorphic rocks of the E-Rhodope, N. Greece:

petrological and geochronological constraints. *Proceedings XV Congress of the Carpathian–Balkan Geological Association, Geological Society of Greece Special Publication,* 4, 602–608.

MUKHOPADHYAY, P.K. (1994) Vitrinite reflectance as maturity parameter: Petrographic and molecular characterization and its applications to basin modeling, in: Mukhopadhyay, P.K., Dow, W.G., (Eds.), Vitrinite Refl ectance as a Maturity Parameter: Applications and Limitations: American Chemical Society, Symposium Series, pp. 1–24.

MUKASA, S., HAYDOUTOV, I., CARRIGAN, C. & KOLCHEVA, K. (2003) Thermobarometry and 40Ar/39Ar ages of eclogitic and gneissic rocks in the Sredna Gora and Rhodope terranes of Bulgaria. *Journal of Czech Geological Society* 48, 94–95.

NESBITT., H.W. & YOUNG., G.M. (1982) Early Proterozoic climates and plate motions inferred from major element chemistry of lutites. *Nature* 299, 715-717.

NESBITT, H.W. & YOUNG, G.M. (1996) Petrogenesis of sediments in the absence of chemical weathering: Effects of abrasion and sorting on bulk composition and mineralogy. *Sedimentology* 43, 341-358.

OVTCHAROVA, M., QUADT, A.V., HEINRICH, C.A., FRANK, M., KAISER-ROHMEIER, M., PEYTCHEVA, I. & CHERNEVA, Z. (2003) Triggering of hydrothermal ore mineralization in the Central Rhodopean Core Complex (Bulgaria): insight from isotope and geochronological studies on tertiary magmatism and migmatisation. In: *Mineral Exploration and Sustainable Development* (Ed D.G. Eliopoulos et al.), 1, 367–370. Millpress, Rotterdam.

PAPADOPOULOS, P. (1982) Geologic map of Greece, Scale 1:50 000, Sheet Maronia. I.G.M.E., Athens.

PE-PIPER, G. & PIPER, D. J. W. (2006) Unique features of the Cenozoic igneous rocks of Greece, in: Dilek, Y., Pavilides, S., (Eds.), Postcollisional tectonics and magmatism in the Mediterranean region and Asia. GSA Special Paper 409, 259-282.

PERRI, F. (2008) Clay mineral assemblage of the Middle Triassic-Lower Jurassic mudrocks from Western-Central Mediterranean Alpine Chains. *Periodico di Mineralogia* 77, 23-40.

PERRI, F. (2014) Composition, provenance and source weathering of Mesozoic sandstones from Western-Central Mediterranean Alpine Chains. *Journal of African Earth Sciences* 91, 32-43.

PERRI, F., RIZZO, G., MONGELLI, G., CRITELLI, S., PERRONE, V. (2008a) Zircon compositions of Lower Mesozoic redbeds of the Tethyan Margins, West-Central Mediterranean area. *International Geology Review* 50, 1022–1039.

PERRI, F., CIRRINCIONE, R., CRITELLI, S.,MAZZOLENI, P. & PAPPALARDO, A. (2008b) Clay mineral assemblages and sandstone compositions of the Mesozoic Longobucco Group (north-eastern Calabria): implication for burial history and diagenetic evolution. *International Geology Review* 50, 1116–1131.

PERRI, F., CRITELLI, S.,MONGELLI, G. & CULLERS, R.L. (2011a) Sedimentary evolution of the Mesozoic continental redbeds using geochemical and mineralogical tools: the case of Upper Triassic to Lowermost Jurassic Monte di Gioiosa mudrocks (Sicily, southern Italy). *International Journal of Earth Sciences* 100, 1569–1587.

PERRI, F., MUTO, F. & BELVISO, C. (2011b) Links between composition and provenance of Mesozoic siliciclastic sediments from Western Calabria (Southern Italy). *Italian Journal of Geosciences* 130, 318–329.

PERRI, F., CRITELLI, S., CAVALCANTE, F., MONGELLI, G., DOMINICI, R., SONNINO, M. & DE ROSA, R. (2012a) Provenance signatures for the Miocene volcaniclastic succession of the Tufiti di Tusa Formation, southern Apennines, Italy. *Geological Magazine*149, 423-442.

PERRI, F., CRITELLI, S., DOMINICI, R., MUTO, F., TRIPODI, V. & CERAMICOLA, S. (2012b) Provenance and accommodation pathways of late Quaternary sediments in the deep-water northern Ionian Basin, southern Italy. *Sedimentary Geology* 280, 244-259.

PERRI, F., CRITELLI, S., MARTÌN-ALGARRA, A., MARTÌN-MARTÌN, M., PERRONE, V., MONGELLI, G. & ZATTIN, M. (2013) Triassic redbeds in the Malaguide Complex (Betic Cordillera – Spain): petrography, geochemistry, and geodynamic implications. *Earth-Science Reviews* 117, 1–28.

PERRI, F., BORRELLI, L., CRITELLI, S. & GULLÀ, G. (2014) Chemical and minero-petrographic features of Plio-Pleistocene fine-grained sediments in Calabria (southern Italy). *Italian Journal of Geosciences* 133, 101–115.

PERRI, F. & OTHA T. (2014) Paleoclimatic conditions and paleoweathering processes on Mesozoic continental redbeds from Western-Central Mediterranean Alpine Chains. *Palaeogeography, Palaeoclimatology, Palaeoecology* 395, 144–157.

PEYTCHEVA, I. & VON QUADT, A. (1995) U–Pb zircon dating of metagranites from Byala-reka region in the east Rhodopes, Bulgaria. *Proceedings XV Congress of the Carpathian–Balkan Geological Association, Geol. Soc. Greece Spec. Publ.,* 4, 637–642.

POLLASTRO, R.M. (1993) Consideration and applications off the illite/smectite geothermometer in hydrocarbon-bearing rocks of Miocene to Mississippian age. *Clays and Clay Minerals* 41, 119-133.

PYTTE, A.M. & REYNOLDS, R.C. JR. (1989) The kinetics of the smectite to illite reaction in contact metamorphic shales, in: Naeser N.D., McCulloch T.H., (Eds.), The termal history of sedimentary basins, Springer-Verlag, New York, pp. 133-140.

SOMELAR, P., KIRSIMAEE, K. & SRODON, J. (2009) Mixed-layer illite-smectite in the Kinnekulle K-bentonite, northern Baltic Basin. *Clay Minerals* 44, 455-468.

TAYLOR, S.R. & MCLENNAN, S.M. (1985) *The Continental Crust: Its Composition and Evolution.* Blackwell, Oxford, United Kingdom.

TSIKOURAS, B. & HATZIPANAGIOTOU, K. (1998) Petrographic evolution of an ophiolite fragment in an ensialic marginal basin, northern Aegean (Samothraki Island, Greece). *European Journal of Mineralogy* 10, 551-567.

TSIKOURAS, B., PE-PIPER, G. & HATZIPANAGIOTOU, K. (1990) A new date for an ophiolite of the northeastern margin of the Vardar zone, Samothraki, Greece. *Neues Jb. Geol. Palaontol. Monat.* 11: 512-527.

TSOKAS, G.N., CHRISTOFIDES, C. & PAPAKONSTANTINOU, C. (1996) A geophysical study of the granites and the sedimentary basins of the Xanthi area (N Greece). *Pure Applied Geophysics* 146, 365–392.

WEIBEL, R. (1999) Effects of burial on the clay assemblages in the Triassic Skagerrak Formation Denmark. *Clay Minerals* 34, 619-635.

YANEV, Y., INNOCENTI, F., MANETTI, P. & SERRI, G. (1998) Upper Eocene-Oligocene collision-related volcanism in Eastern Rhodopes (Bulgaria)-Western Thrace (Greece): petrogenetic affinity and geodynamic significance. *Acta Vulcanologica* 10, 265–277.

ZAGHLOUL, M.N., CRITELLI, S., PERRI, F., MONGELLI, G., PERRONE, V., SONNINO, M., TUCKER, M., AIELLO, M. & VENTIMIGLIA, C. (2010) Depositional systems, composition and geochemistry of Triassic rifted-continental margin redbeds of Internal Rif Chain, Morocco. *Sedimentology* 57, 312-350.

Figure Captions

Fig. 1 – Schematic sketch with the position of the Thrace Basin with respect to the main tectonic units and structures of the eastern Mediterranean region (modified after Kilias *et al.*, 2011)

Fig. 2 – Simplified geological map of the Rhodope province with the location of the studied samples. The Thrace Basin and the other structural units are shown (modified after Kilias *et al.*, 2011).

Fig. 3 – Synthetic and schematic stratigraphic sections with location of the studied samples (modified from Caracciolo *et al.*, 2011b). CRB, Circum-Rhodope Belt; UTU, Upper Tectonic Unit; LTU, Lower Tectonic Unit. The "Evros and southern Thrace stratigraphic scheme" is located in the Evros depocenter (see Fig. 1) and the "Xanthi-Komotini stratigraphic scheme" is located in the Xanthi-Komotini depocenter (see Fig. 1).

Fig. 4 – Exposure of key lithofacies of the stratigraphic sections where the studied samples have been collected. (A) Samotraky section characterized by graded sandstones alternating with mudrocks. (B) Particular of Samotraky section with 10 cm to 50 cm sandstone beds alternating with fine mudrocks. (C) Limnos section characterized by medium to fine-grained stratified sandstones alternating with mudrocks; the lower portion shows soft-sediment deformation structures. (D) Section between Paterma and Organi villages characterized by centimeter-to-meter-thick graded sandstones alternating with siltstones and mudrocks. (E) Section between Paterma and Gratini villages characterized by meter-thick stratified siltstones and mudrocks alternating with thin-bedded fine to medium-grained sandstones. (F) View of the passage from mudrocks and siltstones alternating with centimeter-thick fine-grained sandstones to meter-thick mudrocks and siltstones of the Iasmos section. (G) Coarse-grained sandstone and gravel beds alternating with mudrocks of the Esimi section.

Fig. 5 – (a) Normalization of major and trace elements to upper continental crust averages (after McLennan *et al.* 2006). The plot of the Post-Archean Australian Shales (PAAS; Taylor & McLennan 1985) is shown for comparison. (b) Classification diagram for the studied samples (after Herron, 1988).

Fig. 6 – Decomposition at low angles of the characteristic diffraction profile of ADV, LMN, ES, GRD, PAT, SAMO, IAS and ORG samples (< 2 μm fraction).

Fig. 7 – Vitrinite reflectance determination (R_o% measurement) of the studied samples.

Fig. 8 – (a) Analyzing the provenance by using relations of Cr/V vs. Y/Ni (after Hiscott 1984). Curve model mixing between granite and ultramafic end-members. (b) V-Ni-La*6 ternary diagram, showing fields representative of felsic, mafic and ultramafic rocks plot separately (modified from Perri *et al.*, 2011b).

Fig. 9 – (a) Ternary A-CN-K and A-N-K diagrams. Legend: Ms, muscovite; Ilt, illite; Kln, kaolinite; Chl, chlorite; Gbs, gibbsite; Smt, smectite; Bt, biotite; Kfs, K-feldspar; Pl, plagioclase; A, Al_2O_3; CN, $CaO+Na_2O$; K, K_2O; CIA, Chemical Index of Alteration (modified from Nesbitt & Young, 1982). (b) A-CNK-FM ternary diagram of the studied samples. A, Al_2O_3; CNK, $CaO+Na_2O+K_2O$; FM, Fe_2O_3+MgO. (c) Ternary $15Al_2O_3–300TiO_2–Zr$ plot after García *et al.* (1994), suggesting poor sorting and rapid deposition of the sediments.

Fig. 10 – Schematic sketch of the fault geometry and kinematics and magmatic activity during Paleogene-Neogene extension of Rhodope Massif (modified after Kilias et al., 2011), referred to the Figs. 1 and 2.

Tables

Table 1 – Major and trace elements and ratio values of the studied samples. CIA, Chemical Index of Alteration (Nesbitt & Young, 1982); CIA', Chemical Index of Alteration without CaO values (e.g. Perri *et al.*, 2014); ICV, Index of Compositional Variability (Cox *et al.*, 1995).

Table 2 – Whole rock XRD analyses of the studied samples. Qtz, quartz; Σ Feld (K-feldspars + plagioclase); Pl, plagioclase; K-feld, K-feldspars; Dol, dolomite; Cal, calcite; Σ Phyll, phyllosilicates; Hem, hematite; I-S, illite-smectite mixed layers; Chl-S, chlorite-smectite mixed layers; Kao, kaolinite; Chl, chlorite.

Table 3 – Clay fraction XRD analyses of the studied samples and I/S features and KI. I-S, illite-smectite mixed layers; Chl-S, chlorite-smectite mixed layers; Kao, kaolinite; Chl, chlorite; KI (Kübler Index).

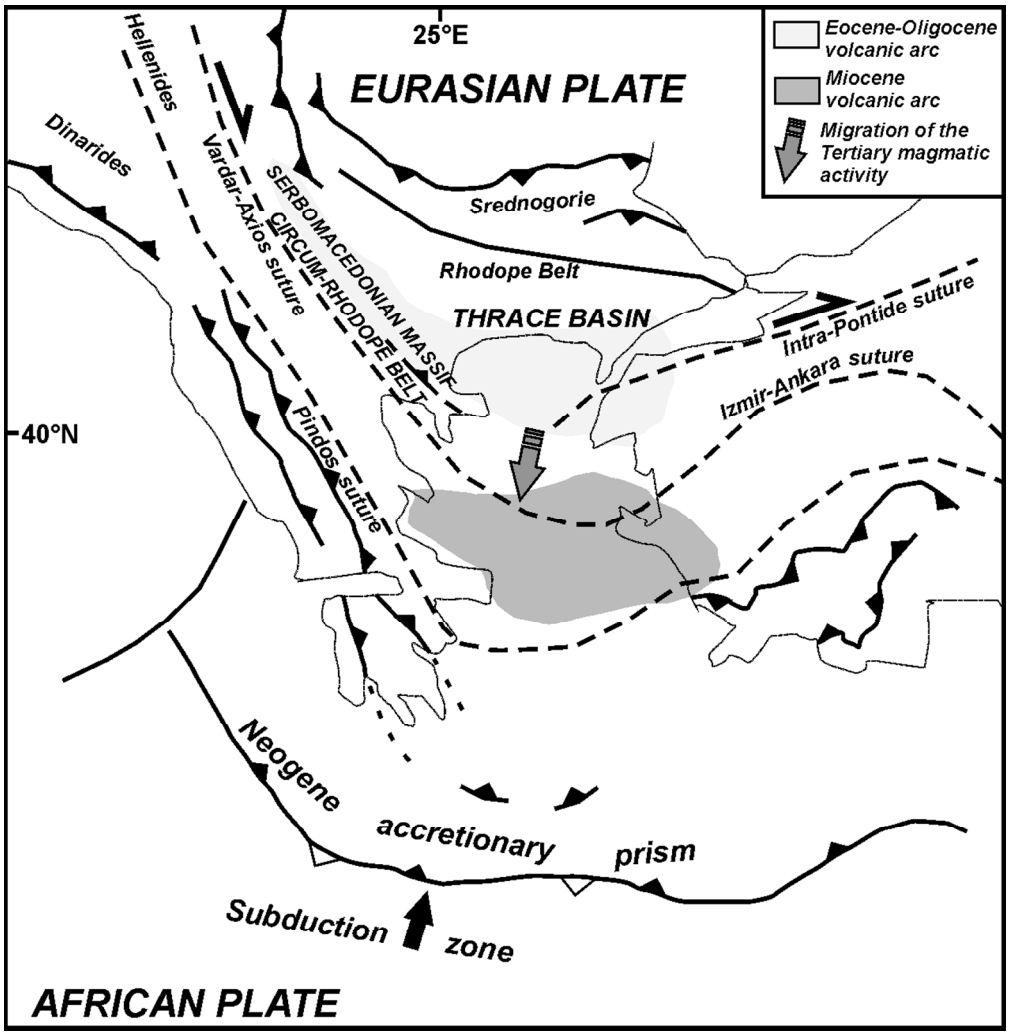

107x110mm (300 x 300 DPI)

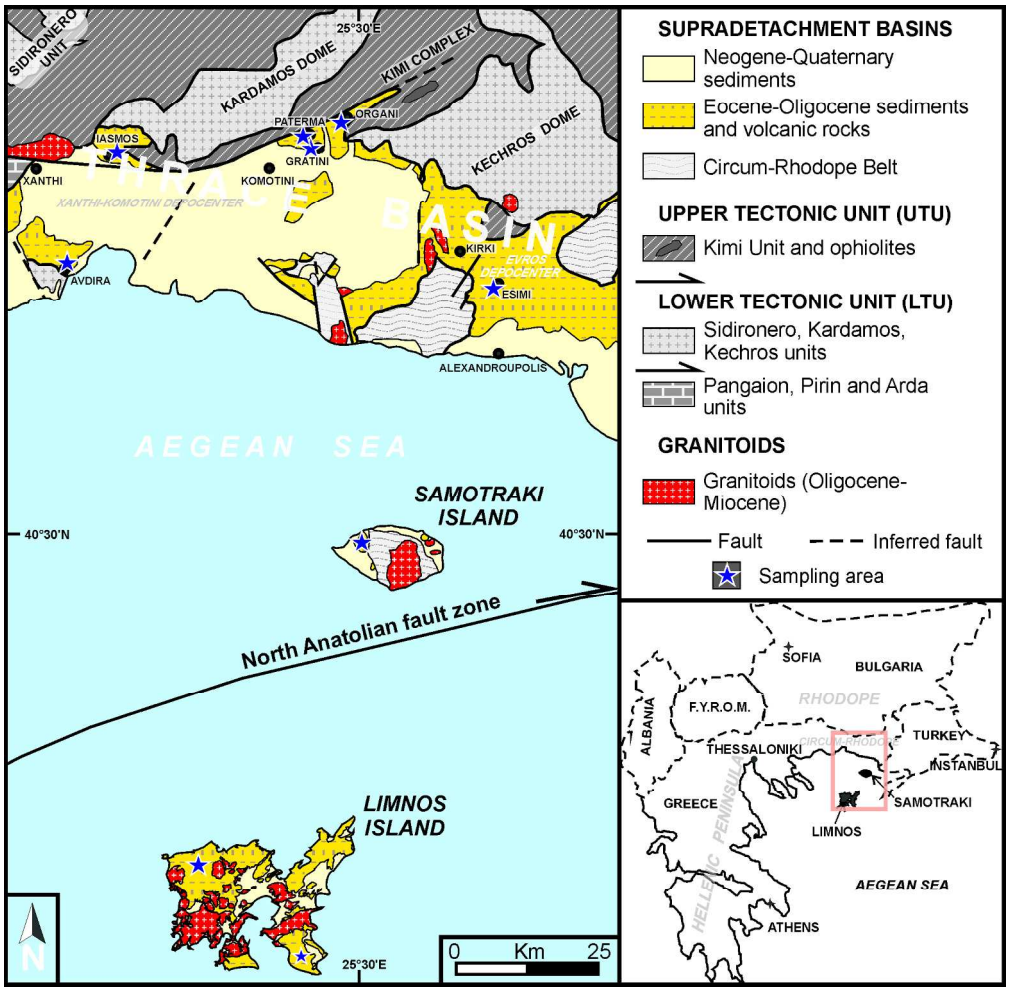

198x194mm (300 x 300 DPI)

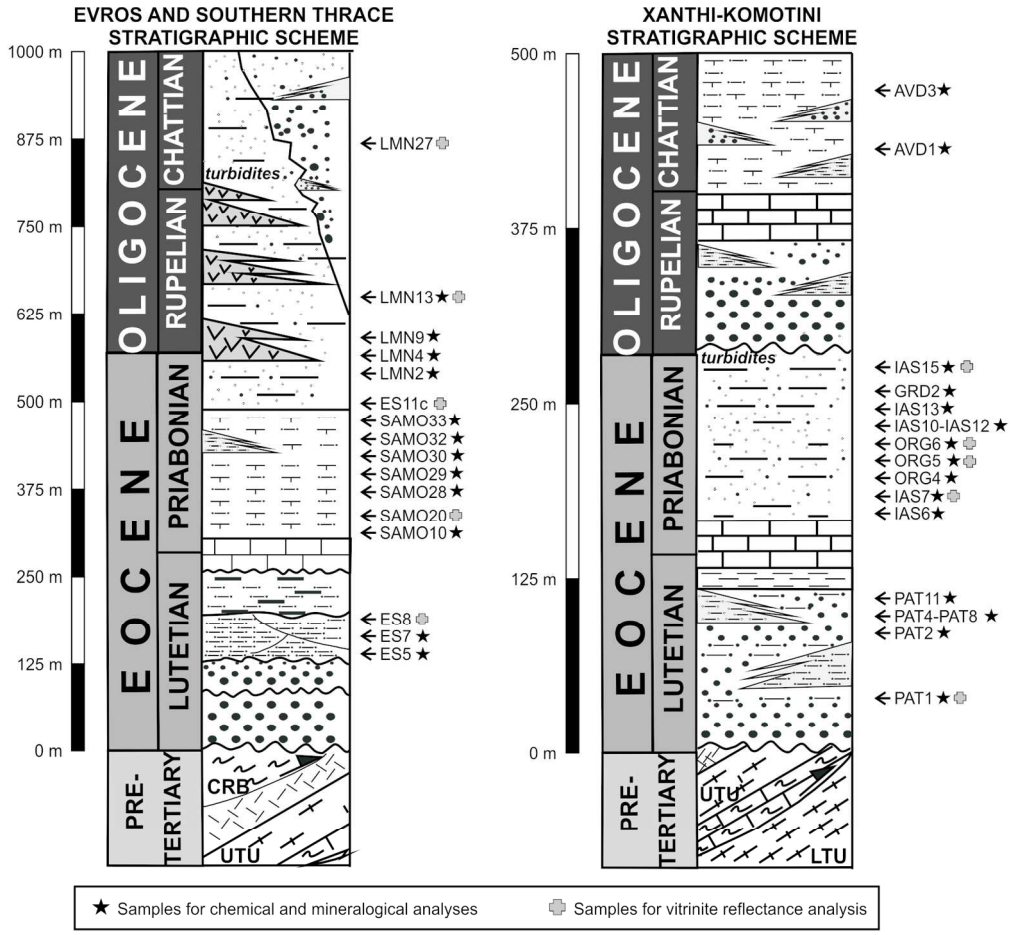

150x138mm (300 x 300 DPI)

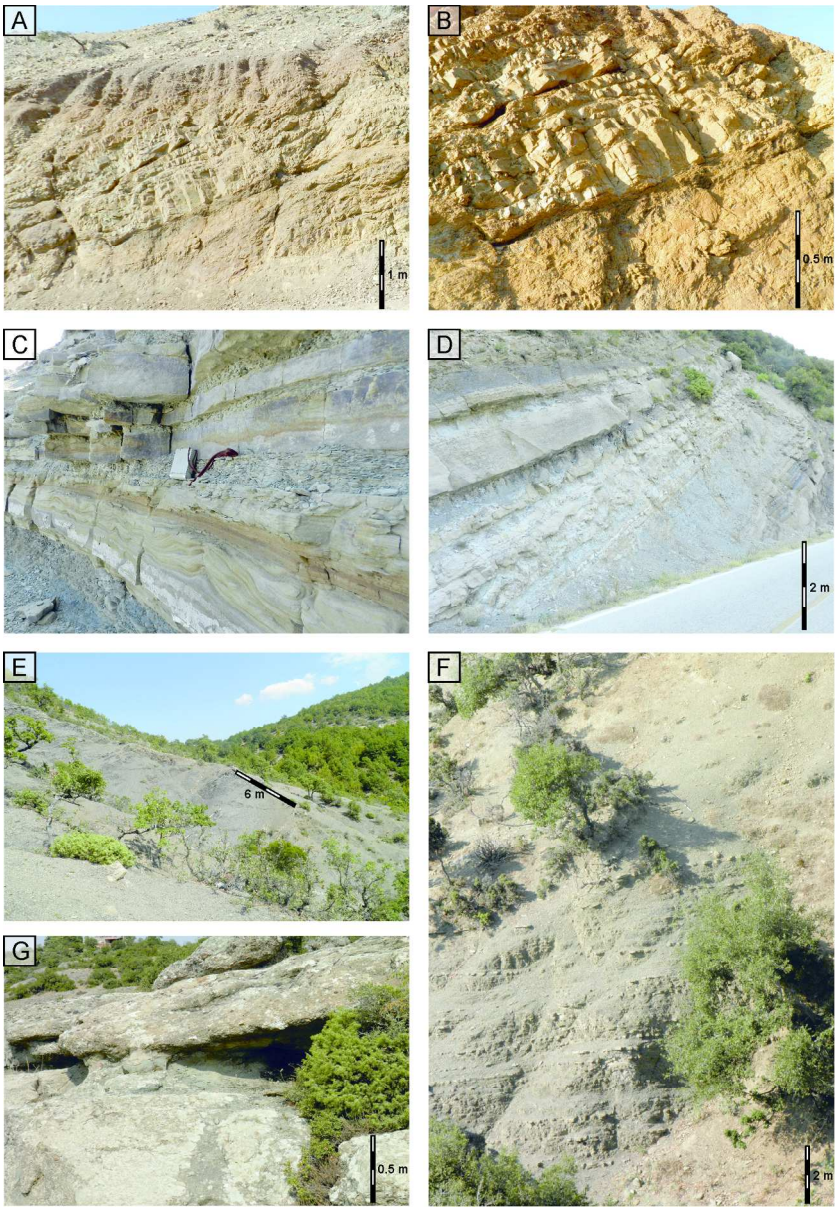

144x208mm (300 x 300 DPI)

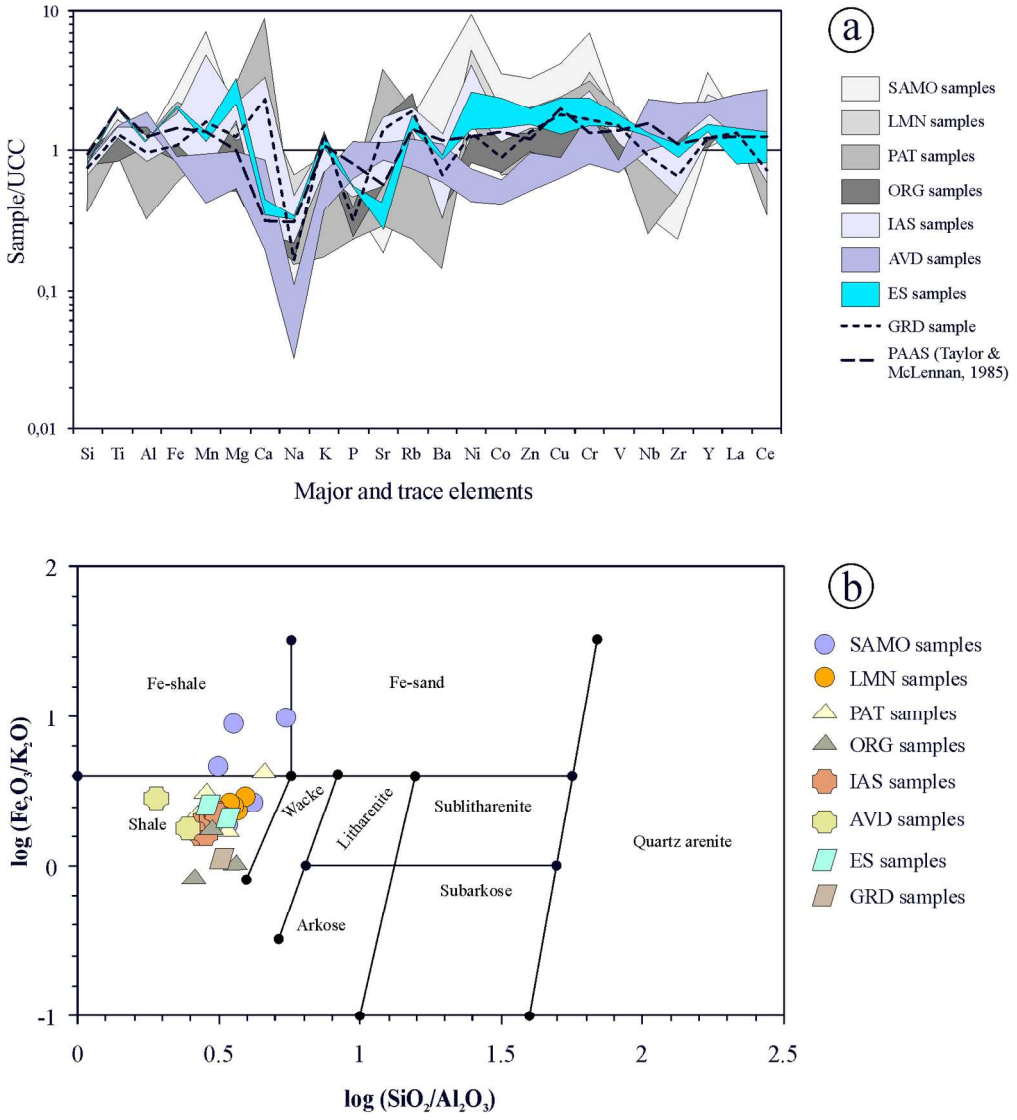

148x164mm (300 x 300 DPI)

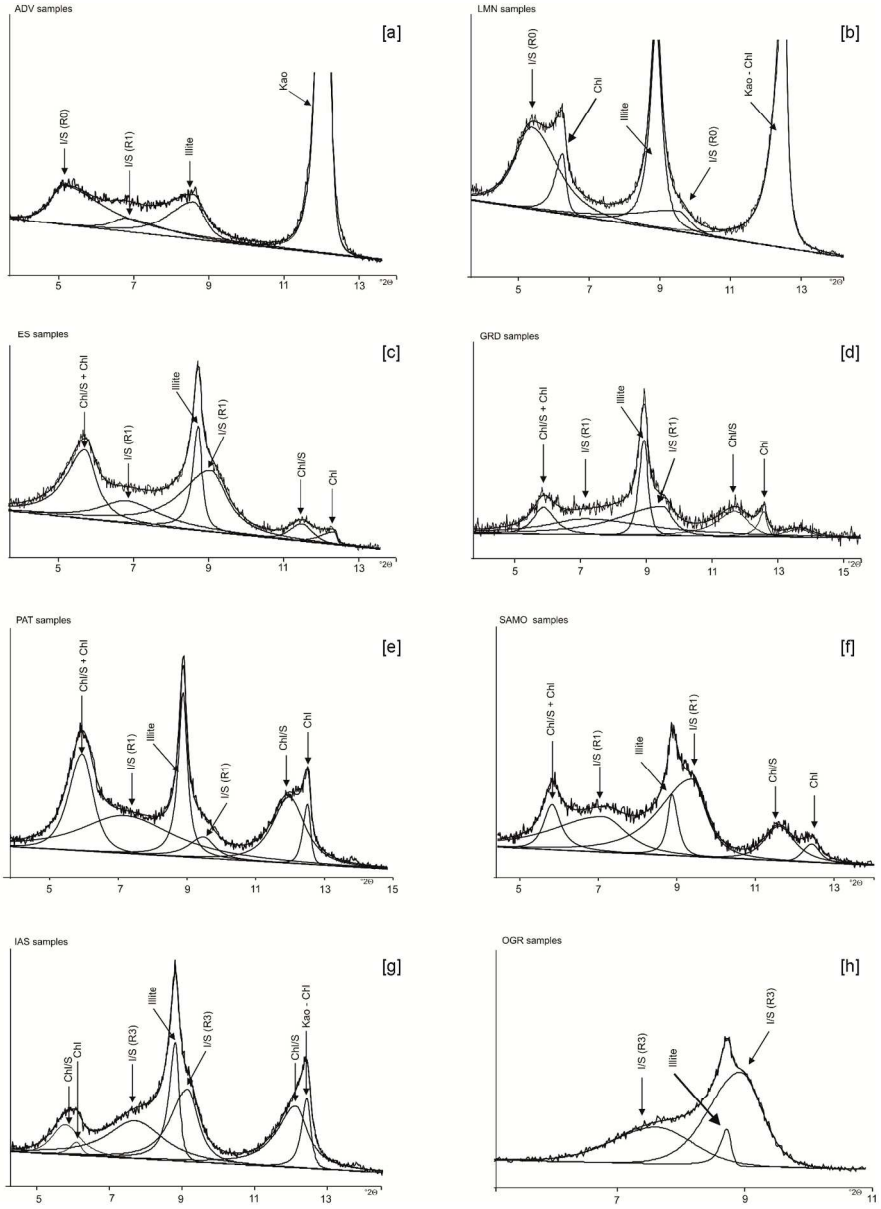

144x193mm (300 x 300 DPI)

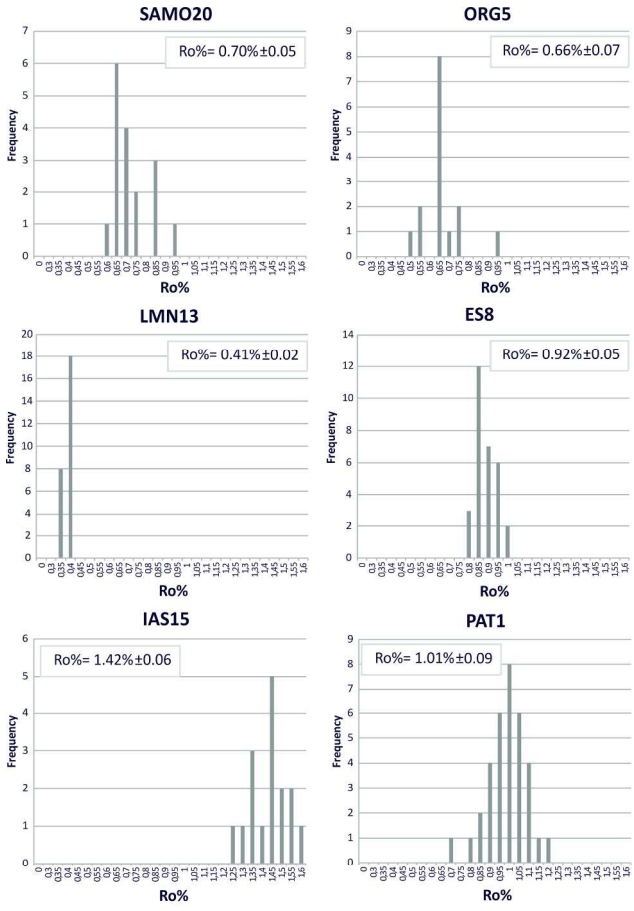

SAMPLE	Ro%	Sd	Nr fragments
SAMO20	0.70	0.05	17
ORG 5	0.66	0.07	14
ORG 6	nd	-	-
LMN 13	0.41	0.02	26
LMN 27	nd	-	-
ES 8	0.92	0.05	30
ES11c	0.49	0.09	15
IAS 7	nd	-	-
IAS 15	1.42	0.06	16
PAT 1	1.01	0.09	34

144x278mm (300 x 300 DPI)

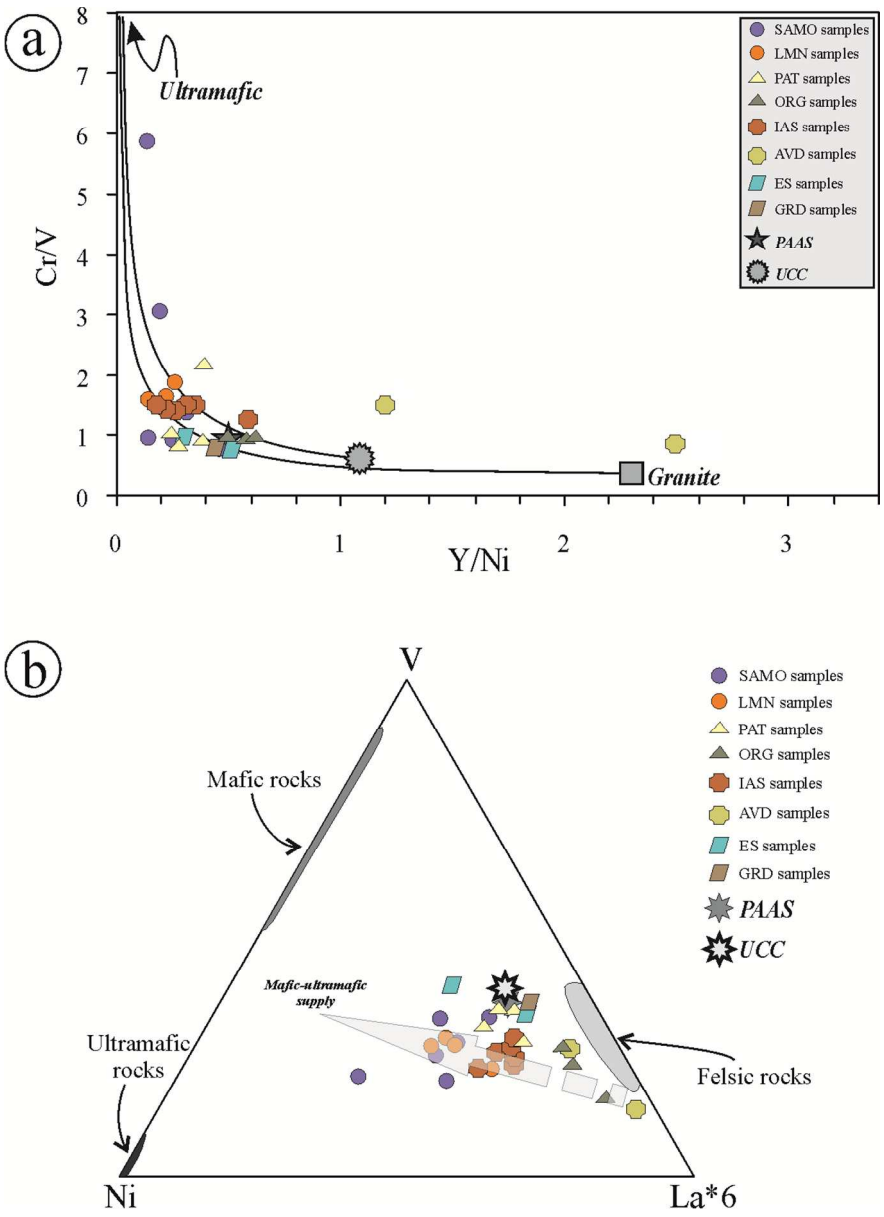

102x141mm (300 x 300 DPI)

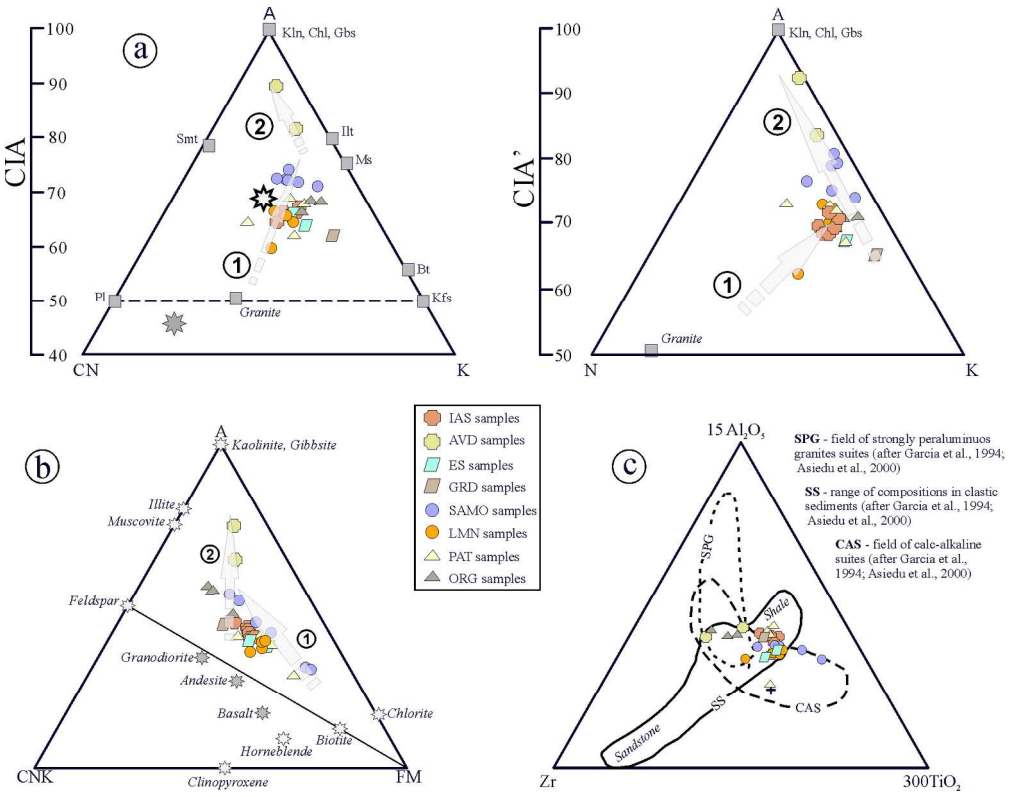

176x137mm (300 x 300 DPI)

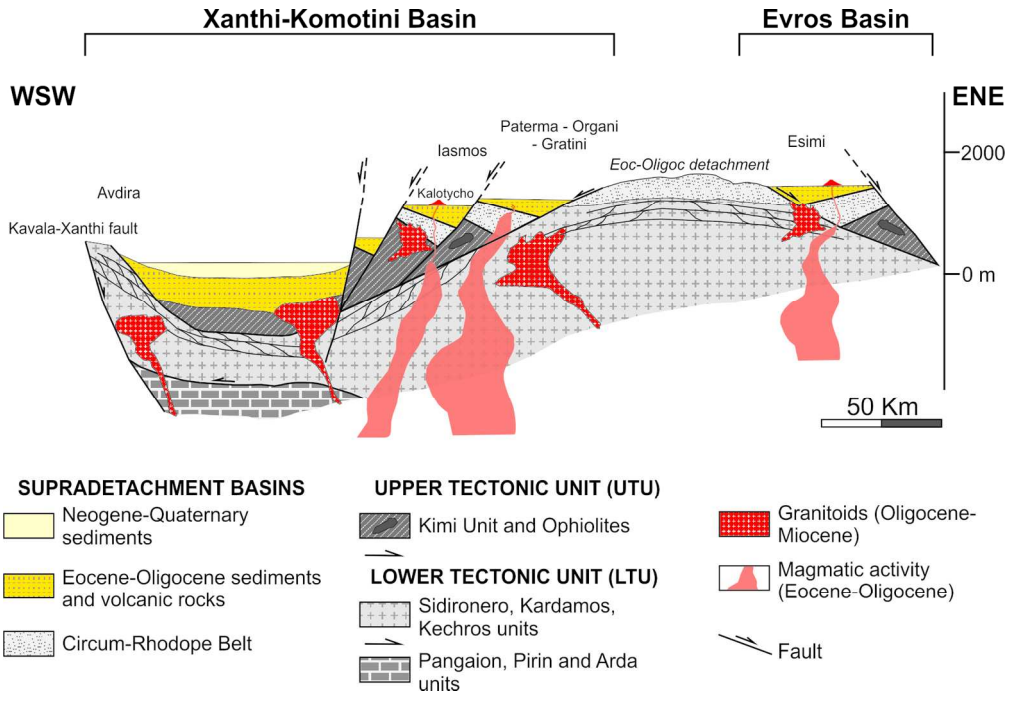

149x101mm (300 x 300 DPI)

Table 1 – Major and trace elements and ratio values of the studied samples. CIA, Chemical Index of Alteration (Nesbitt & Young, 1982); CIA', Chemical Index of Alteration without CaO values (e.g. Perri et al., 2014); ICV, Index of Compositional Variability (Cox et al., 1995).

Samples	SAMO10	SAMO28	SAMO29	SAMO30	SAMO32	SAMO33	LMN2	LMN4	LMN9	LMN13	PAT1	PAT4	PAT8	PAT11
Oxides (wt%)														
SiO_2	51,12	56,02	29,90	66,96	60,86	46,58	52,04	52,83	50,76	52,23	23,54	46,29	51,41	49,76
TiO_2	0,99	0,87	0,68	0,75	0,56	0,97	0,85	0,67	0,85	0,84	0,46	0,60	0,78	0,80
Al_2O_3	17,82	16,54	8,27	15,49	9,71	14,49	14,30	12,95	13,73	14,39	4,82	13,10	17,91	18,84
Fe_2O_3	7,81	4,74	10,50	5,28	12,86	9,25	7,53	6,32	7,34	6,99	2,60	5,32	10,04	8,76
MnO	0,05	0,12	0,57	0,03	0,14	0,22	0,06	0,07	0,07	0,07	0,08	0,15	0,10	0,07
MgO	3,82	1,39	1,50	1,50	1,92	2,27	5,26	4,82	5,25	5,37	5,15	3,39	6,70	5,89
CaO	5,32	6,64	25,43	2,52	4,66	10,48	4,74	8,17	7,21	6,49	36,54	12,48	1,65	2,52
Na_2O	0,37	0,77	0,15	1,09	0,15	0,40	2,60	0,98	1,08	0,93	0,59	0,98	1,08	0,83
K_2O	3,54	2,74	1,20	1,99	1,30	2,05	3,14	2,19	2,96	2,68	0,58	3,14	3,12	3,84
P_2O_5	0,08	0,12	0,15	0,11	0,19	0,15	0,10	0,10	0,11	0,10	0,08	0,10	0,05	0,09
LOI	8,76	9,57	21,58	4,28	6,94	13,04	9,00	10,98	9,76	9,92	25,30	13,67	6,44	8,68
Total	99,68	99,53	99,93	100,00	99,30	99,90	99,64	100,08	99,12	100,02	99,75	99,22	99,28	100,09
Trace elements (ppm)														
V	195	140	191	98	173	179	188	123	180	162	115	163	202	209
Cr	191	433	154	579	170	261	305	234	280	256	266	170	186	231
Co	21	23	61	22	57	35	33	19	20	29	12	19	32	29
Ni	120	188	170	170	414	183	233	138	189	174	70	73	106	147
Rb	196	135	72	81	70	110	164	101	149	136	26	191	189	222
Sr	168	136	233	65	65	94	174	392	225	211	1333	469	102	145
Y	31	37	80	23	58	57	33	37	36	35	30	31	30	37
Zr	148	148	44	169	93	94	123	186	131	148	91	106	140	125
Nb	16	12	4	8	7	8	12	12	11	11	3	8	12	13
Ba	489	290	346	226	262	203	311	351	287	327	79	387	443	424
La	49	41	40	40	45	50	49	51	46	46	40	42	47	55
Ce	79	64	38	57	36	58	69	61	59	60	22	44	49	73
Cu	38	41	104	28	37	38	42	28	43	43	31	54	57	61
Zn	125	70	234	57	138	102	130	89	108	99	51	101	115	145
Ratios														
CIA	71	72	73	73	75	73	60	67	65	68	64	62	69	68
CIA'	75	76	80	77	81	79	63	73	69	72	74	68	74	72
ICV	1,23	1,04	4,77	0,85	2,21	1,75	1,69	1,79	1,80	1,62	9,52	1,98	1,31	1,20

Samples	GRD2	ORG4	ORG5	ORG6	IAS6	IAS7	IAS10	IAS12	IAS13	IAS15	AVD1	AVD3	ES5	ES7
Oxides (wt%)														
SiO_2	50,18	66,49	51,08	58,93	44,24	48,93	55,65	54,18	47,32	51,13	53,94	56,22	51,62	53,83
TiO_2	0,65	0,42	0,56	0,72	0,62	0,67	0,80	0,82	0,82	0,82	0,73	0,76	0,99	1,04
Al_2O_3	14,54	16,99	16,29	22,23	12,78	12,97	19,53	18,68	13,85	15,89	28,64	22,43	17,73	18,03
Fe_2O_3	4,93	3,74	5,65	3,78	4,97	5,67	6,49	8,22	6,47	7,14	3,61	4,07	9,40	8,88
MnO	0,13	0,08	0,16	0,04	0,09	0,09	0,06	0,06	0,39	0,18	0,03	0,04	0,11	0,09
MgO	2,75	1,13	2,59	1,65	3,62	4,16	4,15	5,02	4,54	4,72	1,19	2,17	7,27	4,75
CaO	9,89	1,32	6,02	0,84	14,21	11,23	1,55	1,04	10,71	6,75	0,81	3,61	1,46	1,87
Na_2O	0,63	0,64	1,28	1,32	0,84	1,26	1,84	1,55	1,01	1,23	0,13	0,42	1,30	1,24
K_2O	4,42	3,76	3,35	4,60	2,64	2,44	3,98	3,92	2,63	3,29	1,27	2,35	3,55	4,32
P_2O_5	0,06	0,05	0,07	0,08	0,10	0,10	0,12	0,10	0,14	0,09	0,13	0,23	0,11	0,11
LOI	11,48	5,23	12,71	5,49	15,17	11,79	5,78	5,96	11,62	8,58	8,93	7,58	5,78	5,78
Total	99,67	99,84	99,76	99,68	99,29	99,31	99,95	99,55	99,50	99,81	99,40	99,87	99,32	99,95
Trace elements (ppm)														
V	162	81	125	137	124	121	145	148	152	149	75	91	192	158
Cr	138	84	120	134	190	187	226	226	198	216	67	153	193	126
Co	15	12	22	16	20	23	23	25	22	25	7	10	40	25
Ni	59	36	54	48	84	99	134	183	94	136	19	32	117	63
Rb	216	224	197	284	163	158	223	227	154	198	83	134	160	198
Sr	493	246	577	197	538	601	246	197	529	444	299	392	93	145
Y	27	23	33	24	30	30	26	38	56	33	50	40	33	30
Zr	125	216	181	266	90	110	173	154	147	136	421	219	165	211
Nb	11	16	13	19	9	11	16	16	10	13	28	12	15	16
Ba	369	210	237	234	179	332	689	716	397	480	325	595	476	506
La	40	61	60	53	42	48	61	57	48	53	77	38	24	43
Ce	47	97	78	88	38	45	92	77	63	62	176	60	53	87
Cu	45	20	42	27	36	37	38	39	44	46	15	22	58	33
Zn	97	70	94	86	113	128	128	137	102	126	37	68	140	110
Ratios														
CIA	62	68	67	69	67	65	65	66	66	65	90	82	66	64
CIA'	65	71	70	71	71	70	69	69	72	70	93	84	71	68
ICV	1,60	0,65	1,19	0,58	2,11	1,96	0,96	1,10	1,89	1,51	0,27	0,60	1,35	1,23

Table 2 – Whole rock XRD analyses of the studied samples. Qtz, quartz; Σ Feld (K-feldspars + plagioclase); Pl, plagioclase; K-feld, K-feldspars; Dol, dolomite; Cal, calcite; Σ Phyll, phyllosilicates; Hem, hematite; I-S, illite-smectite mixed layers; Chl-S, chlorite-smectite mixed layers; Kao, kaolinite; Chl, chlorite.

Sample	I-S	Chl-S	Illite/ mica	Kao	Chl	Qtz	K-feld	Pl	Cal	Dol	Hem	Σ Phyll	Σ Feld
ADV1	8	0	3	61	1	21	3	2	1	0	0	73	5
ADV3	20	0	3	24	1	33	5	8	5	0	0	50	13
ES5	2	5	20	4	14	28	1	25	0	0	0	46	26
ES7	19	4	20	0	4	23	6	23	tr	0	1	46	29
GRD2	18	6	21	0	3	27	2	6	17	0	0	48	8
IAS6	10	2	13	3	10	25	0	8	22	7	1	38	9
IAS7	10	0	6	2	6	35	1	20	20	0	0	24	21
IAS10	12	3	12	2	7	31	5	28	1	tr	0	35	33
IAS12	15	3	12	3	7	31	6	24	0	0	0	40	29
IAS13	6	1	5	1	3	35	4	27	19	tr	0	16	30
IAS15	8	1	19	0	10	28	3	18	11	tr	1	39	22
LMN2	21	tr	25	2	14	27	0	3	7	0	0	62	3
LMN4	36	tr	21	0	6	20	0	7	10	0	0	63	7
LMN9	13	tr	28	0	10	27	2	9	11	0	0	51	11
LMN13	9	1	10	3	8	42	2	15	10	tr	0	32	16
ORG4	26	0	27	0	0	40	1	4	1	0	0	53	6
ORG5	25	0	21	0	0	29	1	10	0	15	0	46	10
ORG6	0	0	61	0	0	30	0	9	0	0	0	61	9
PAT1	2	5	2	0	1	12	3	12	64	tr	0	10	15
PAT4	8	4	12	2	7	36	0	11	21	tr	0	33	11
PAT8	6	13	20	0	18	29	1	13	tr	tr	0	57	14
PAT11	16	0	28	5	12	26	0	11	3	tr	0	60	11
SAMO10	9	7	26	4	7	34	0	3	9	0	0	54	3
SAMO28	15	0	29	0	8	36	0	4	8	0	0	52	4
SAMO29	14	3	10	0	6	17	0	0	45	0	5	33	0
SAMO30	28	0	11	1	5	40	0	12	2	0	1	45	12
SAMO32	8	2	11	3	13	53	0	0	8	0	3	37	0
SAMO33	33	9	8	0	7	22	0	1	16	0	4	57	1

Table 3 – Clay fraction XRD analyses of the studied samples and I/S features and KI. I-S, illite-smectite mixed layers; Chl-S, chlorite-smectite mixed layers; Kao, kaolinite; Chl, chlorite; KI (Kübler Index).

Sample	I-S	Chl-S	Illite	Kao	Chl	I-S features		KI
						Reichweite (Stacking order)	% illite	
ADV1	25	0	6	67	1	R0	40	n. d.
ADV3	49	0	1	44	6	R0	n. d.	n. d.
ES5	25	6	32	6	31	n. d.	n. d.	0,45
ES7	65	18	16	0	1	R1	75	n.d.
GRD2	67	7	23	0	3	R1	80	n. d.
IAS6	n. d.	n. d.	n. d.	n. d.	n. d.	n. d.	n. d.	n. d.
IAS7	50	5	20	6	19	R3	85-90	n. d.
IAS10	74	0	15	3	8	R3	85-90	n. d.
IAS12	70	4	13	4	9	R3	85-90	n. d.
IAS13	57	7	22	4	10	R3	85-90	n. d.
IAS15	64	4	15	0	17	R1	80	n. d.
LMN2	47	8	38	1	7	R0	55-60	n. d.
LMN4	66	5	25	0	3	R0	40	n. d.
LMN9	52	6	34	0	7	R0	50	n. d.
LMN13	39	0	38	6	17	R0	40	n. d.
ORG4	97	0	3	0	0	R3	85-90	n. d.
ORG5	87	0	13	0	0	R3	85	n. d.
ORG6	67	0	33	0	0	n. d.	n. d.	0,56
PAT1	43	17	28	0	11	R1	75-80	n. d.
PAT4	56	15	26	0	3	R1	80-85	n. d.
PAT8	56	12	25	0	7	R1	85	n. d.
PAT11	n. d.	n. d.	n. d.	n. d.	n. d.	n. d.	n. d.	n. d.
SAMO10	19	8	69	2	3	n. d.	n. d.	0,44
SAMO28	65	5	27	0	3	R1	80-85	n. d.
SAMO29	58	13	22	0	7	R1	80-85	n. d.
SAMO30	n. d.	n. d.	n. d.	n. d.	n. d.	n. d.	n. d.	n. d.
SAMO32	19	32	26	5	18	n. d.	80-85	n. d.
SAMO33	69	17	10	0	3	R1	75-80	n. d.